



ELSEVIER

Comput. Methods Appl. Mech. Engrg. 136 (1996) 59–92

**Computer methods
in applied
mechanics and
engineering**

On the solution of mode jumping phenomena in thin-walled shell structures

Eduard Riks^{a,*}, Charles C. Rankin^b, Francis A. Brogan^b

^a*Delft University of Technology, Faculty of Aerospace Engineering, Kluyverweg 1, NL-2600 GB Delft, The Netherlands*

^b*Lockheed Martin, 3251 Hanover Street, Palo Alto, CA 94304-1192, USA*

Received 17 March 1995; revised 6 October 1995

Abstract

This paper is an investigation into the merits of an hybrid procedure for the numerical simulation of transient buckling problems. The procedure consists of the combination of a classical path-following method with a transient integration method where the first method is used for the quasi static (stable) parts of the simulation and the second method for the parts of the simulation that belong to the transient domain. It is shown that the success of the procedure is guaranteed by a proper formulation of the so-called matching conditions that define the transition from one mode of operation to the other.

The chosen strategy turns out to be very robust and it has as an added advantage that it can be applied with relative ease. The power of the approach is demonstrated with the presentation of two simulations: The mode jumping problem of a plate strip and the collapse of a thin-walled composite cylinder in compression.

1. Introduction

The term 'mode jumping' is often used to describe sudden dynamic changes in the wave number, mode shape of the buckled state of a structure during the (quasi static) loading process. These phenomena have been observed to occur in stiffened plate structures. For example, in 1959, M. Stein [1, 2] described a buckling experiment on a plate supported by multiple longitudinal fixtures (see Fig. 1). The experiment was designed with the aim to study the buckling behavior of the skin of a stiffened panel that is loaded in compression. During the experiment, changes in the number of buckles occurred when the equilibrium state of the specimen entered the post-buckling range. The changes in mode shapes occurred in a violent manner and were observed to go from 5 to 6 to 7 to 8 buckles (= half waves measured in the axial direction). The load vs. end-shortening diagram recorded during the experiments was qualitatively of the type pictured in Fig. 2, which corresponds to the case where the experiment is carried out under end-shortening control. Note that the jumps are represented by the vertical arrows in the diagram.

The observed phenomena were analyzed and interpreted by several authors [3–7]. The studies revealed that the plate exhibits a wealth of post-buckling equilibrium states but that only a few of these are stable at a particular value of the load. When the loading is increased, equilibrium is maintained along the stable part of the (current) post-buckling path, the now unstable state. The structure will then move away from this state and enter a transient motion. This motion is the actual jump that enables the structure to reach a new stable equilibrium state corresponding to a different deformation mode. Once the new stable state is reached, the load can further be increased until another point of instability is

* Corresponding author.

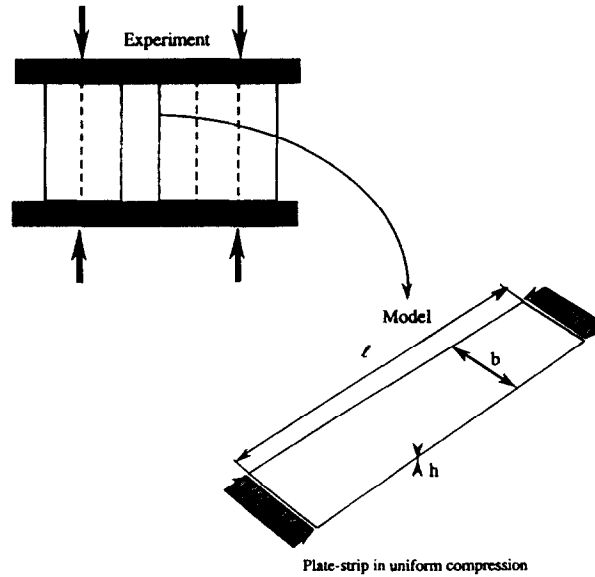


Fig. 1. M. Stein's buckling experiment.

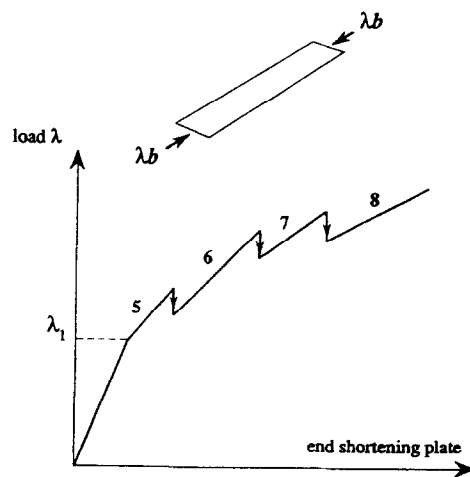


Fig. 2. Load–displacement relation.

encountered. When that occurs, a second mode jump will result. In principle, it is possible that many jumps occur depending on the particulars of the problem.

The authors of the cited references did not address the actual transient process that is so characteristic of these problems. In their treatment of the problem connected with the plate-buckling experiment they confined themselves to the study of the post-buckling states and their stability characteristics. In this manner, a qualitative explanation of the jumping phenomena could be obtained. But the practising engineer faced with the evaluation of the post-buckling strength of stiffened panels is not primarily concerned with the analysis of the many post-buckling equilibrium paths that exist for a specific case. His immediate interest is focused on the determination of the response of the structure to the loads that are applied to it, in a form that clearly reveals when the load carrying capacity is exhausted.

When the structure is more complicated than the plate example mentioned previously, the ways to obtain this information are limited. Experiments are prohibitively expensive and analytical methods ineffective. The only possible affordable way is to perform computer simulations of the behavior of the structure with the help of a shell finite element code. It is then imperative that these simulations should

be able to record diagrams of the type that are given in Fig. 2, i.e. they should be able to approximate the behavior that would be observed in an actual experiment.

Mode jumping problems are transient response problems as far as the jumps are concerned. In between the jumps, the behavior of the structure is governed by stable equilibrium states. But the (stable) paths that the structure follows before and after the jump are not always statically connected with each other (by unstable equilibrium paths). This implies that a quasi static solution method, like the path-following method, is not sufficient by itself to obtain the desired response of the structure. What is needed in this case is either a solution strategy that is entirely based on transient response techniques or a strategy that combines the strength of the static path-following technique with transient response methods. In this paper, we will investigate the merits of the latter approach using standard solution techniques that are available in general purpose finite element codes.

2. Quasi static and transient response

2.1. The governing equations

It is assumed that the shell models studied here are based on a Lagrangian description. The discretized equations of motion are then considered in the form

$$\mathbf{M}\ddot{\mathbf{d}} + \mathbf{D}\dot{\mathbf{d}} + \mathbf{f}(\mathbf{d}; \lambda) = 0 \quad (1a)$$

$$\mathbf{f} = \mathbf{f}^{(i)}(\mathbf{d}) + \mathbf{f}^{(e)}(\mathbf{d}; \lambda)^1 \quad (1b)$$

where

- \mathbf{d} = the set (or vector) of active nodal degrees of freedom, that describes the configuration of the structure.
- $\dot{\mathbf{d}}, \ddot{\mathbf{d}}$ = are the first and second time derivatives, $d/dt, d^2/dt^2$, of these freedoms, i.e. the velocity and acceleration distribution of material points of the shell.
- λ = a load intensity parameter.
- \mathbf{M} = the (positive definite) mass matrix
- \mathbf{D} = the damping matrix
- \mathbf{f} = the set of non-linear functions of the nodal freedoms and the load parameter λ that describe the internal stiffness of the structure $\mathbf{f}^{(i)}$ and the action of the external loads $\mathbf{f}^{(e)}$.

The load intensity is defined by $\mathbf{b} = \lambda \mathbf{b}_0$ where \mathbf{b}_0 denotes a unit or nominal set of externally applied loads that is acting on the structure (dead loads, pressure loads or prescribed displacements or a combination thereof). This loading system generates the load vector $\mathbf{f}^{(e)}(\mathbf{d}; \lambda)$ in Eq. (1b) which is a non-linear function of λ in general, so that $\mathbf{f}(\mathbf{d}; \lambda)$ can be considered to be non-linear in \mathbf{d} as well as in λ . Eqs. (1) represents a wide class of problems. For example, one can think of shells modeled in a small strain, large displacement and rotation theory.

Please note that with the introduction of the vectors \mathbf{d}, \mathbf{f} and the matrices \mathbf{M}, \mathbf{D} in Eq. (1), we have followed a convention whereby bold faced lower case letters denote vectors while bold faced upper case letters stand for matrices. The dimension of the vector of nodal freedoms is: $\text{Dim}(\mathbf{d}) = N$ where $N \gg 1$. The dimension of the other objects is: $\text{Dim}(\mathbf{M}) = N \times N$; $\text{Dim}(\mathbf{D}) = N \times N$; $\text{Dim}(\mathbf{f}) = N$. In many practical problems N is large, say 1000 to 100 000 or possibly more. It is finally noted that the damping \mathbf{D} is taken into account to serve two purposes: To let the simulation be as close as possible to the actual behavior

¹ The notation: $\mathbf{f}(\mathbf{d})$ with \mathbf{d} between skew brackets is used to indicate that \mathbf{f} is a function of \mathbf{d} . The brackets $()$, $[\]$ and $\{ \}$ will be used to group objects in the usual way.

of the structure and to make sure that convergence to a new stable state after a jump will actually take place.

2.2. Quasi static response

The equations of motion govern the dynamic behavior of the shell models. But if the loads are applied slowly in time, the time dependent quantities in (1) are negligible and can be set to zero. This is the notion of quasi static behavior and it is determined by the static equilibrium equations

$$\mathbf{f}(\mathbf{d}; \lambda) = 0 \quad (2)$$

We will assume that the structural models studied here are pseudo conservative, i.e. in spite of the damping introduced in (1) these equilibrium equations are derivable from a potential energy function

$$P = P(\mathbf{d}; \lambda) \quad (3a)$$

so that they follow from the statement

$$\delta \mathbf{d}^T \mathbf{f}(\mathbf{d}; \lambda) = \frac{\partial P}{\partial \mathbf{d}} \delta \mathbf{d} = \mathbf{P}_d \delta \mathbf{d} = 0 \quad (3b)$$

where $\delta \mathbf{d} \neq 0$ denotes any arbitrary virtual displacement. Note that this notation implies

$$\frac{\partial P}{\partial \mathbf{d}} \delta \mathbf{d} = \frac{\partial P}{\partial d_i} \delta d_i \quad (\text{summation over } i); \quad d_i = \mathbf{d}^T \mathbf{e}_i$$

where \mathbf{e}_i ($i=1, 2, \dots, N$) stand for the base vectors that span the N -dimensional space R_N in which \mathbf{d} is described. The notation $\mathbf{d}^T \mathbf{f}$ is the usual notation for the inner product. It also follows from (3) that $\mathbf{f} = (\partial P / \partial \mathbf{d})^T = (\mathbf{P}_d)^T$.

Classical buckling theory focuses exclusively on the analysis and solution of these non-linear equations. If there is only one load parameter λ , as it is assumed here, the equations determine one-dimensional curves in the space R_{N+1} spanned by \mathbf{d} and λ . The geometrical properties of this space curve are related to the stability or instability of the various equilibrium states and this implies that in many cases the load-carrying capacity of a structure can simply be deduced from the form of the solutions of the equilibrium equations.

The solutions \mathbf{d} of the static equation (2) can be written in the parametric form (as a function of λ)

$$\mathbf{d} = \mathbf{d}(\lambda) \in R_N \quad (4)$$

or they can be represented by

$$\mathbf{x} = \begin{Bmatrix} \mathbf{d}(s) \\ \lambda(s) \end{Bmatrix} \in R_{N+1} \quad (5)$$

Here, (s) is a suitable path parameter for example the arc length of the path defined by Eq. (2). The latter form, in shorthand written as $\mathbf{x} = \mathbf{x}(s)$, is more general and often more convenient so that we will make use of it whenever the need arises.

Note that Eq. (2) is defined in such a way that the unloaded state is given by

$$\mathbf{d} = \mathbf{d}(\lambda = 0) = \mathbf{0} \quad \text{or} \quad \mathbf{x} = \begin{Bmatrix} \mathbf{d}(0) \\ \lambda(0) \end{Bmatrix} = \mathbf{0} \quad (6)$$

When the load is slowly increased, the successive deformation states of the structure will be described by a curve (5) that is connected with (6). This path is called the fundamental or primary path

$$\mathbf{x}_1 = \mathbf{x}_1(s) = \begin{Bmatrix} \mathbf{d}(s) \\ \lambda(s) \end{Bmatrix}_1; \quad \text{LIM}_{s \rightarrow 0} \{\mathbf{x}_1(s)\} = \mathbf{0} \quad (7)$$

The study of the stability of this path is a principal goal in classical stability theory. But in this paper, we will also consider equilibrium paths that are not connected with $\mathbf{x}_1(s)$, i.e. curves $\{\mathbf{x}_i(s); i=2, 3, \dots\}$

that have no point in common with $x_1(s)$. Mode jumping can often be seen as the transient behavior of the structure between two of these ‘isolated’ equilibrium paths.

2.3. The dynamic part of the solution

If the structure is loaded in a quasi static fashion as described previously, it will first respond by following the solution path (7) (for increasing values of λ) and this process can be continued until the stability of the solutions is lost. At that particular point, $s=s_c$, or instant $t=t_0$, the static response of the structure will change into a dynamic response governed by Eq. (1). This response corresponds to an orbit that can be written in the parametric form:

$${}^1x(t) = {}^1 \left\{ \begin{matrix} d(t) \\ \lambda(t) \end{matrix} \right\} \quad t_0 < t < \infty \tag{8}$$

where t denotes the time, t_0 =the time at the start of the motion. It can thus also be seen as a space curve in R_{N+1} . In this paper it will be assumed that an orbit of this nature will always have a begin point and an (different) end point, denoted by: ${}^1x(t_0)$, ${}^1x(\infty)$, respectively. The starting point corresponds to the configuration at which stability of the equilibrium solution (7) was lost. The endpoint is the solution of (1) at which the motion comes to a rest, i.e. ${}^1\dot{d}(\infty) = {}^1\ddot{d}(\infty) = 0$, and this is a configuration that must necessarily correspond to a stable equilibrium state (Fig. 3).

For practical reasons, the orbits that will be encountered are supposed to have a finite length which is associated with a finite duration $\Delta t = t_r - t_0$, in contrast to what is suggested at (8). The time t_r is then determined by our notion of rest. The structure will have attained a state of rest (= stable equilibrium) when for any $t > t_r$, $\|{}^1\dot{d}(t)\| < \varepsilon$, where ε is a preset, small positive number, and $\|\cdot\|$ denotes a suitable vector norm. Because the kinetic energy is a positive definite quadratic form of the velocities, it is useful to take the kinetic energy $T_2({}^1\dot{d}(t))$ for the norm $\|\cdot\|^2$, i.e. $\|{}^1\dot{d}(t)\|^2 = T_2({}^1\dot{d}(t))$ (see Section 5.6). The motion (8) is then considered to be terminated at $t = t_r$ when

$$t_r: T_2({}^1\dot{d}(t)) < \varepsilon^2 \quad \text{for } \forall t > t_r \tag{9a}$$

This definition implies that the configuration ${}^1x(t_r)$ is so close to ${}^1x(\infty)$ that we can assume that

$${}^1x_r = {}^1x(t_r) \approx {}^1 \left\{ \begin{matrix} d(\infty) \\ \lambda(\infty) \end{matrix} \right\} \tag{9b}$$

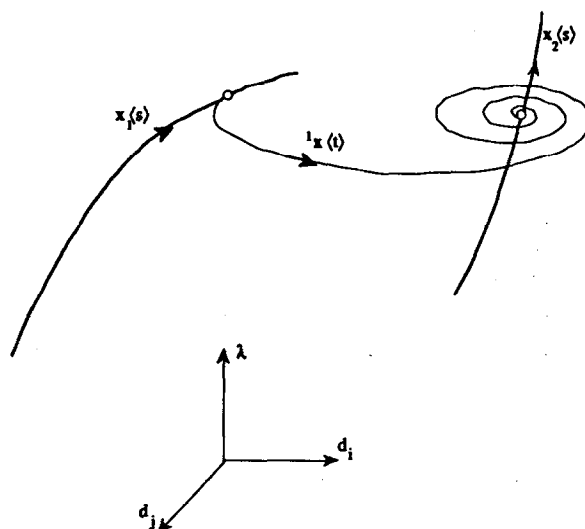


Fig. 3. Heteroclinic orbit.

2.4. The transition problem

In the real world, the transition from static to dynamic behavior that takes place at the point where stability is lost is an inevitable outcome of the conditions to which the structure is subjected. The structure experiences always very small random motions around the current equilibrium state as a result of its interaction with its natural surroundings. These induced disturbances will (eventually) guide the structure into the jumping motion as soon as the point of loss of stability is reached.

However, the situation is different when one wants to simulate this transition process numerically. In that case it is not sufficient to start the computations from the point at which stability loss occurs, even when one applies a small arbitrarily chosen initial motion as an initial condition. As we will explain in the sequel, this follows because it is not possible to guarantee that such arbitrary, but nevertheless particular choice of the initial disturbance will result in the expected jumping motion within an acceptable period of computation time. In the numerical simulation it turns out to be necessary to make use of the circumstance that the jumping motion can only occur along predetermined directions. The initial (or transition) conditions should therefore be chosen accordingly.

3. A summary of classical results

3.1. Necessary and sufficient conditions, critical points

To bring our analysis into perspective, we first summarize the conditions that determine the stability of the equilibrium solutions of (2). The most popular test for stability in elasticity is the energy criterion. This criterion concerns the behavior of conservative systems at equilibrium states determined by Eq. (2). An equilibrium state of an elastic structure under conservative loading conditions is stable if and only if the potential energy of this system is a proper minimum at that state. If this condition is not satisfied, the system is unstable [8–10].

Thus, an equilibrium state \mathbf{d} is stable if and only if the potential energy function $P\langle \mathbf{d}; \lambda \rangle$ satisfies

$$P\langle \mathbf{d} + \delta \mathbf{d}; \lambda \rangle - P\langle \mathbf{d}; \lambda \rangle > 0 \quad (10)$$

for $\forall \delta \mathbf{d} \neq 0 \in R_N$ (again, δ is here the usual symbol for a virtual variation).

But in this general form, the energy criterion (attributed to Lagrange and Dirichlet) is difficult to use. It is much more practical to apply a weaker form of (10). The weaker form of the energy criterion concerns the properties of the so-called second variation of the potential energy, the quadratic form

$$\Pi_2 = \delta \mathbf{d}^T P_{dd} \delta \mathbf{d} = \delta \mathbf{d}^T \mathbf{K}^T \delta \mathbf{d} = \delta \mathbf{d}^T \mathbf{K} \delta \mathbf{d} \quad (11)$$

which is built on the Jacobian $\mathbf{K}\langle \mathbf{d}; \lambda \rangle$ of the equations of equilibrium (2). \mathbf{K} is thus defined by

$$\mathbf{K} = \mathbf{K}\langle \mathbf{d}; \lambda \rangle = \mathbf{f}_d\langle \mathbf{d}; \lambda \rangle = \frac{\partial \mathbf{f}\langle \mathbf{d}; \lambda \rangle}{\partial \mathbf{d}} = (P_{dd})^T \quad (12)$$

Note that the dimension of \mathbf{K} is $N \times N$ and that we use the notation for the derivative of \mathbf{f} with respect to \mathbf{d} as $\mathbf{f}_d = (\partial \mathbf{f}\langle \mathbf{d}; \lambda \rangle / \partial d_i) \mathbf{e}_i^T$ (sum over i) where $\{\mathbf{e}_i\}$ ($i=1, 2, \dots, N$) are the natural or (computation-al) base vectors that define \mathbf{d} : $\mathbf{d} = d_i \mathbf{e}_i$ (sum over i).

At a solution point of (2) the derivative \mathbf{K} is the system's stiffness matrix. It is always symmetric in the cases considered here, thus $\mathbf{K} = \mathbf{K}^T$. Well known is the sufficient condition for stability on the basis of \mathbf{K} : An equilibrium state: $\mathbf{x} = (d_1, d_2, \dots, d_N, \lambda)^T = (\mathbf{d}^T, \lambda)^T$ is stable if \mathbf{K} is positive definite or if

$$\text{for } \forall \delta \mathbf{d} \neq 0 \quad \delta \mathbf{d}^T \mathbf{K}\langle \mathbf{x} \rangle \delta \mathbf{d} > 0 \quad (13a)$$

The equilibrium state \mathbf{x} is unstable if \mathbf{K} is indefinite, or if

$$\delta \mathbf{d}^T \mathbf{K}\langle \mathbf{x} \rangle \delta \mathbf{d} < 0 \quad (13b)$$

for some $\delta \mathbf{d} \neq 0$. In the discrete setting in which we are presenting our analysis, condition (13a) and

(13b) are sufficient conditions for the existence or absence of a minimum of the potential energy. Because they are much easier to verify than (11), conditions (13) are very useful in practical computations.

In between (13a) and (13b) one possibility still remains. This occurs when \mathbf{K} becomes semi positive definite and the quadratic form on \mathbf{K} satisfies

$$\delta \mathbf{d}^T \mathbf{K} \langle \mathbf{x} \rangle \delta \mathbf{d} \geq 0 \quad \text{for } \forall \delta \mathbf{d} \neq 0 \quad (14)$$

The equality sign holds here for at least one direction $\delta \mathbf{d}$. In this case, the configuration \mathbf{x} at which \mathbf{K} is evaluated is called a critical state. In what follows we will denote such a special point by \mathbf{x}_c or $[\mathbf{d}_c^T, \lambda_c]^T$. By critical is meant that \mathbf{x}_c may or may not be stable because when (11) holds stability is no longer determined by the properties of \mathbf{K} alone. In this special case, it is only the strong form of the energy criterion can decide the matter [8–10].

Thus, any configuration $\mathbf{x} = \mathbf{x}_c$ that satisfies (14) is called a critical state. In many cases, a critical state \mathbf{x}_c marks the boundary between a stable and an unstable part of the equilibrium path.² This occurs when the stability of an equilibrium state $\mathbf{x} \langle s \rangle$ that passes through \mathbf{x}_c changes. When the change of stability occurs along a curve $\mathbf{x} \langle s \rangle$ at $\mathbf{x}_c = \mathbf{x} \langle s_c \rangle$ (defined by (14)) the state $\mathbf{x}_{c-} = \mathbf{x} \langle s_c - \varepsilon \rangle$, ($\varepsilon > 0$) just before \mathbf{x}_c satisfies (13a) and the state just after $\mathbf{x}_{c+} = \mathbf{x} \langle s_c + \varepsilon \rangle$ also belonging to $\mathbf{x} \langle s \rangle$ satisfies (13b) no matter how small ε is chosen. It is this phenomenon of change of stability that is of special interest in this paper.

The energy criterion as it is presented here is the discrete analog of the energy criterion for continuous systems. It can be brought into relation with the dynamic criterion of stability of Liapounov which is based on the dynamic analysis of the effect of small disturbances around an equilibrium state [8–10]. In Section 4 we will give this criterion a mechanical interpretation. But first we continue with the introduction of some additional concepts that are useful in this investigation.

3.2. Limit points and bifurcation points

We will now restrict our considerations to critical states $\mathbf{x}_c = \mathbf{x} \langle s_c \rangle$ that belong to a special case of (14), i.e. the case that there is only *one* direction that leads to the equality sign in (14). The eigenvalues and eigenvectors of $\mathbf{K} \langle \mathbf{x}_c \rangle = \mathbf{K}^T \langle \mathbf{x}_c \rangle$ then obey the conditions

$$\begin{aligned} \text{(i)} \quad & \mathbf{K} \langle \mathbf{x}_c \rangle \mathbf{a} \langle i \rangle - \omega \langle i \rangle \mathbf{a} \langle i \rangle = 0 \\ \text{(ii)} \quad & \omega \langle 1 \rangle = 0; \quad \omega \langle i \rangle > 0; \quad i = 2, 3, 4, \dots \\ \text{(iii)} \quad & \mathbf{a} \langle i \rangle^T \mathbf{a} \langle j \rangle = \delta_{ij} \quad (\delta_{ij} = \text{Kronecker symbol}) \end{aligned} \quad (15)$$

Note that for convenience we impose a normalization on the eigen modes $\mathbf{a} \langle i \rangle$ of \mathbf{K} (iii). The null vector $\mathbf{a} \langle 1 \rangle$ of the singular $\mathbf{K} \langle \mathbf{x}_c \rangle$ is called the (critical) buckling mode and in the following we will always denote this mode simply by \mathbf{a} . It plays a dominant role in the discussions that follow.

Condition (15) defines the simplest possible case of a critical state that can occur. Consequently, such states are referred to as simple critical points. We will now investigate in what way the solutions of (2) manifest themselves in the neighborhood of these points. The geometrical form of the solutions near \mathbf{x}_c can be analyzed by considering the Taylor expansion

$$\mathbf{x} \langle s_c + \Delta s \rangle = \mathbf{x} \langle s_c \rangle + \mathbf{x}' \langle s_c \rangle \Delta s + \frac{1}{2} \mathbf{x}'' \langle s_c \rangle \Delta s^2 + \dots \quad (16)$$

where as before $()' = d()/ds$ and s = the arclength of $\mathbf{x} \langle s \rangle$. However, here we will restrict our attention to the first characteristic property of the curve (16). This is the first path derivative $\mathbf{x}' \langle s_c \rangle$, the (unit)

² An example of a path through a critical state that does not change stability is given by the branch 2 of a pitchfork bifurcation shown in Fig. 4(c,d).

tangent to the path at x_c . The study of the equations that determine $x'(s_c)$ make it possible to distinguish between two classes of simple critical points: Limit points and Bifurcation points.

The equations that determine $x'(s_c)$ are given by

$$\begin{aligned} \text{(i)} \quad f_x(x_c)x' &= 0 \rightarrow K(d_c, \lambda_c)d' + f_\lambda(d_c, \lambda_c)\lambda' = 0; \quad (K = f_d) \\ \text{(ii)} \quad x'^T x' &= 1 \rightarrow d'(d_c, \lambda_c)^T d'(d_c, \lambda_c) + \lambda'(d_c, \lambda_c)\lambda'(d_c, \lambda_c) = 1 \end{aligned} \quad (17)$$

These equations are obtained by differentiation of (2) with respect to s along $x(s)$. Please note that Eq. (17ii) is the condition that enforces the path parameter s to be the arclength of $x(s)$ at s_c .

At the critical states considered here the Jacobian K is singular as described by (15). Consequently, the solution of Eq. (17i) only exists if $\text{Rank}(K) = \text{Rank}(K^*) = N-1$, where K^* stands for the augmented matrix $K^* = [K; f_\lambda]$. Another way of saying this is that the vector $f_\lambda \lambda'$ must be in the range of K . This conclusion then leads to the observation that

$$a^T f_\lambda \lambda' = 0 \quad (18)$$

There are thus two possible types of solution for x' at the critical point x_c . One type is associated with $\lambda'_c = 0$ the other with $(a^T f_\lambda)_c = 0$.

(I) In the first situation (17i) reduces to

$$\begin{aligned} K(d_c, \lambda_c)d' &= 0 \\ d'^T d' &= 1 \end{aligned} \quad (19a)$$

As follows from the definition (15), this set of equations has a unique solution

$$d'_c = a = a(1) \quad (19b)$$

so that at a critical point where

$$\lambda'_c = 0; \quad (a^T f_\lambda)_c \neq 0, \quad (20)$$

we deal with a stationary point with respect to the direction e_{N+1} , the base vector associated with the load parameter λ . In many cases, condition (20) will indicate the existence of a limit point because it represents one of the conditions that mark a *limit point*

$$\begin{aligned} x'_c &= \frac{dx(s_c)}{ds} = \text{single valued} \\ \lambda'_c &= \frac{d\lambda(s_c)}{ds} = 0; \quad \lambda''_c = \frac{d^2\lambda(s_c)}{ds^2} < 0 \end{aligned} \quad (21)$$

Note that at a limit point, the buckling mode a represents the tangent to the critical state $x(s_c)$. We mention this property here because it makes the practical formulation of the jump conditions at limit points relatively easy (see Section 5).

REMARK. Because (19a) determines the tangent x'_{c1} apart from its sign, i.e. $d'_c = a(1)$ and $d'_c = -a(1)$ are both solutions, it is useful to introduce a convention that fixes the sign of d'_c . Thus, to avoid confusion the tangent is determined in such a way that it points in the direction of the *unstable* part of the branch $x_1(s)$ beyond $x_1(s_c)$. The condition for d'_c that corresponds to this choice is then given by

$$d'^T_c f_\lambda(x_c) < 0 \quad (22)$$

(II) We now return to the second possibility when $(a^T f_\lambda)_c = 0$. In that case Eq. (17) is solved by

$$\begin{aligned} d' &= d'_{1,2} = z + \alpha_{1,2}a \\ \lambda &= \lambda'_{1,2} \end{aligned} \quad (23)$$

Here, z is a particular solution of (17i) and $\alpha_{1,2}$ stands for two constants which are not determined by

(17) but by the second order derivative of Eq. (2). The description of the way these solutions can be obtained in this case is of no particular interest at this point. It is therefore deferred to Appendix A.

Thus, if the condition

$$\lambda'_c \neq 0; \quad (\mathbf{a}^T \mathbf{f}_\lambda)_c = 0 \quad (24)$$

applies, we have in general an indication that the critical state defined by (14) is a *bifurcation point*. The solutions for the tangents at \mathbf{x}_c are then

$$\mathbf{x}'_c = \frac{d\mathbf{x}}{ds} = \text{multiple valued} = \mathbf{x}'_{c1}, \mathbf{x}'_{c2} \quad (25)$$

A simple critical state is thus either a stationary (or limit) point, *or*, it is a bifurcation point. However, the reverse is not true. Limit points and bifurcation points that are encountered in the solutions of (2) are not automatically critical states in the sense discussed here. They are only critical if the second variation satisfies (14) thus when \mathbf{K} is semi-positive definite (see also Appendix A).

The classification of the character of the solutions of Eq. (2) in the neighborhood of \mathbf{x}_c (that we started by considering the solution of the path derivative \mathbf{x}'_c), can be continued with the study of the curvature terms \mathbf{x}''_{c1} , \mathbf{x}''_{c2} , etc. but this avenue will not be pursued here. Instead, we will introduce another way of looking at the local solutions around \mathbf{x}_c which is not based on the explicit character of the expansion (16), but on the specific properties of the governing equations that generate these path derivatives. This is a classification that focuses on the so-called reduced form of the equilibrium equation (2), a transformation that is produced by the Liapounov–Schmidt reduction method [6, 7] or, similarly, by the variational version of this method developed by Koiter [8, 9] (see also [10, 11]). This reduced form of Eq. (2) plays a crucial role in the selection of the transition conditions to be discussed later in Section 5.3. To clarify this role, it is necessary to consider this transformation and subsequently have a close look at the results it produces in a number of cases.

3.3. Liapounov–Schmidt–Koiter reduction

Again, we study critical states \mathbf{x}_c characterized by condition (15). To study the form of the solution $\mathbf{x}(s)$ of (2) in the neighborhood of \mathbf{x}_c it is advantageous to introduce the composition

$$\begin{aligned} \mathbf{d} &= \mathbf{d}_c + \Delta \mathbf{d}; & \Delta \mathbf{d} &= \mu \mathbf{a} + \mathbf{v}; & \mathbf{a}^T \mathbf{v} &= 0 \\ \lambda &= \lambda_c + \Delta \lambda \end{aligned} \quad (26)$$

where μ measures the participation of \mathbf{a} in $\Delta \mathbf{d}$ and \mathbf{v} is an additional vector that must be determined to complete the solution $\Delta \mathbf{d}$. By this ‘change of basis’ the solution is decomposed into two terms, one in the direction of the ‘buckling mode’ \mathbf{a} and the other in a direction perpendicular to \mathbf{a} anticipating that close to the critical point the solution $\Delta \mathbf{d}$ must be dominated by \mathbf{a} .

We recall that the equilibrium equations given at (2) are considered to be derived from the potential energy function $P(\mathbf{d}; \lambda)$ (Eqs. (3)). With the new variable μ and the constraint on \mathbf{v} introduced at (25) we can reformulate these equations by considering the modified potential

$$P^* = P(\mathbf{d}_c + \Delta \mathbf{d}; \lambda) + \omega \mathbf{a}^T \mathbf{v} \quad (27)$$

where ω is a Lagrange multiplier that is introduced to enforce $\mathbf{a}^T \mathbf{v} = 0$. The stationary value of this modification with respect to μ , \mathbf{v} and ω is determined by the variational equation

$$[P_d \langle \mathbf{d}_c + \Delta \mathbf{d}; \lambda \rangle \mathbf{a}] \delta \mu + [P_d \langle \mathbf{d}_c + \Delta \mathbf{d}; \lambda \rangle + \omega \mathbf{a}^T] \delta \mathbf{v} + [\mathbf{a}^T \mathbf{v}] \delta \omega = 0 \quad (28a)$$

which, in terms of \mathbf{f} yields the $N+2$ dimensional set of equilibrium equations

$$\begin{aligned} \text{(i)} \quad & \mathbf{a}^T \mathbf{f} \langle \mathbf{d}_c + \mu \mathbf{a} + \mathbf{v}; \lambda_c + \Delta \lambda \rangle = 0 \\ \text{(ii)} \quad & \mathbf{f} \langle \mathbf{d}_c + \mu \mathbf{a} + \mathbf{v}; \lambda_c + \Delta \lambda \rangle + \omega \mathbf{a} = \mathbf{0} \\ \text{(iii)} \quad & \mathbf{a}^T \mathbf{v} = 0 \end{aligned} \quad (28b)$$

This extended set of equations in the unknowns μ , ω and \mathbf{v} is completely equivalent to the original equation (2). The transformed set can be seen as the composition of the projection of \mathbf{f} to the complement of the range of (\mathbf{K}) (i), and the projection of \mathbf{f} to the range of (\mathbf{K}) (ii). By this modification, the splitting of the equations into a singular and a regular part can be achieved. The first part is singular with respect to μ at \mathbf{x}_c but the second part is still regular. It can be solved uniquely for \mathbf{v} in the near neighborhood of \mathbf{x}_c because it can be shown that the Jacobian of (ii) is non-singular in this neighborhood.

Eq. (32ii) determines \mathbf{v} , ω as a function of μ and λ . Assuming that it is possible to construct the solution $\mathbf{v} = \mathbf{V}\langle\mu, \Delta\lambda\rangle$ (for small $\Delta\lambda, \mu$) one can substitute it in (i) and obtain

$$\begin{aligned} g\langle\mu, \Delta\lambda\rangle &= 0 \\ g &= \mathbf{a}^T \mathbf{f}\langle\mathbf{d}_c + \mu\mathbf{a} + \mathbf{V}\langle\mu, \Delta\lambda\rangle; \lambda_c + \Delta\lambda\rangle \end{aligned} \quad (29)$$

What remains is then the determination of the solution of (29).

Eq. (29) is the reduced equation in the Liapounov–Schmidt–Koiter reduction method. Sometimes it is referred to as the fundamental bifurcation equation. In our case of a simple critical point, it is a single equation and its significance is that all the essential information pertaining to the behavior of the solutions near the critical points \mathbf{x}_c is contained in it. To see this we need to develop the perturbation or asymptotic solutions of (28) around \mathbf{x}_c .

3.4. Perturbation solutions

Expansion of Eqs. (28) and (29) in terms of μ and $\Delta\lambda$, makes it possible to unveil the general characteristics of the solutions in the near neighborhood of \mathbf{x}_c . To support the discussion in Sections 4 and 5, we shall summarize the most important results that have been obtained on the basis of this type of analysis. To shorten the notation, we will make use of the definitions

$$\underline{f} = \mathbf{f}\langle\mathbf{d}_c; \lambda_c\rangle; \quad \underline{f}_d = \mathbf{f}_d\langle\mathbf{d}_c; \lambda_c\rangle; \quad \underline{f}_\lambda = \mathbf{f}_\lambda\langle\mathbf{d}_c; \lambda_c\rangle; \quad \underline{f}_{dd} = \mathbf{f}_{dd}\langle\mathbf{d}_c; \lambda_c\rangle; \quad \text{etc.} \quad (30)$$

The underscore thus indicates that the function \mathbf{f} and subsequent derivatives \mathbf{f}_d , \mathbf{f}_{dd} , etc. are evaluated at the critical state \mathbf{x}_c under investigation. Note that \underline{f}_λ denotes: $\underline{f}_\lambda = \partial\mathbf{f}/\partial\lambda$ and that $\underline{f}_d \mathbf{d} = \partial\mathbf{f}/\partial d_i d_i$; $\underline{f}_{dd} \mathbf{d} \mathbf{d} = \partial\mathbf{f}/\partial^2 d_i d_j d_i d_j$, etc.

The leading terms in Eq. (29) can then be written as

$$\begin{aligned} g\langle\mu, \Delta\lambda\rangle &= \mathbf{a}^T \left[\underline{f}_d(\mu\mathbf{a} + \mathbf{V}) + \underline{f}_\lambda \Delta\lambda \right] + \frac{1}{2} \underline{f}_{dd}(\mu\mathbf{a} + \mathbf{V})(\mu\mathbf{a} + \mathbf{V}) + 2 \underline{f}_{d\lambda}(\mu\mathbf{a} + \mathbf{V}) \Delta\lambda + \underline{f}_{\lambda\lambda} \Delta\lambda^2 \\ &\quad + \frac{1}{3!} \underline{f}_{ddd} \mu^3 + \text{HOT} \end{aligned}$$

With use of the identity $\mathbf{a}^T \underline{f}_d(\mu\mathbf{a} + \mathbf{V}) = 0$, this is simplified to

$$\begin{aligned} g\langle\mu, \Delta\lambda\rangle &= \mathbf{a}^T \underline{f}_\lambda \Delta\lambda + \frac{1}{2} \{ \mathbf{a}^T \underline{f}_{dd} \mu\mu + 2 \mathbf{a}^T \underline{f}_{dd} \mathbf{a} \mathbf{V}\langle\mu, \Delta\lambda\rangle \mu \\ &\quad + \mathbf{a}^T \underline{f}_{dd} \mathbf{V}\langle\mu, \Delta\lambda\rangle \mathbf{V}\langle\mu, \Delta\lambda\rangle + 2 \mathbf{a}^T \underline{f}_{d\lambda} \mu \Delta\lambda \\ &\quad + 2 \mathbf{a}^T \underline{f}_{d\lambda} \mathbf{V}\langle\mu, \Delta\lambda\rangle \Delta\lambda + \mathbf{a}^T \underline{f}_{\lambda\lambda} \Delta\lambda^2 \} + \frac{1}{3!} \mathbf{a}^T \underline{f}_{ddd} \mu^3 + \text{HOT} \end{aligned} \quad (31)$$

It can now easily be seen that for small μ and $\Delta\lambda$, the solution of (28ii) is qualitatively of the form

$$\mathbf{v} = \mathbf{V}\langle\mu, \Delta\lambda\rangle = \mathbf{w}_{10} \Delta\lambda + \mathbf{w}_{20} \Delta\lambda^2 + \mathbf{w}_{11} \mu \Delta\lambda + \mathbf{w}_{02} \mu^2 \quad (32)$$

because linearization of (28ii) gives

$$\begin{aligned} \underline{f}_d \mathbf{v} + \omega \mathbf{a} &= -\mathbf{f}\langle\mathbf{d}_c + \mu\mathbf{a}, \lambda_c + \Delta\lambda\rangle \\ \mathbf{a}^T \mathbf{v} &= 0 \end{aligned}$$

or

$$\begin{aligned} \underline{f}_d \mathbf{v} + \omega \mathbf{a} &= -\underline{f}_\lambda \Delta\lambda - \frac{1}{2} [\underline{f}_{dd} \mathbf{a} \mathbf{a} \mu^2 + 2 \underline{f}_{d\lambda} \mathbf{a} \mu \Delta\lambda + \underline{f}_{\lambda\lambda} \Delta\lambda^2] + \text{HOT} \\ \mathbf{a}^T \mathbf{v} &= 0 \end{aligned} \quad (33)$$

Once the solution $\mathbf{v} = \mathbf{V}$ is obtained, it is possible to write

$$\begin{aligned} \mathbf{V}^T \underline{f}_d \mathbf{V} &= -\mathbf{V}^T \underline{f}_\lambda \Delta\lambda - \frac{1}{2} \mathbf{V}^T [\underline{f}_{dd} \mathbf{a} \mathbf{a} \mu^2 + 2 \underline{f}_{d\lambda} \mathbf{a} \mu \Delta\lambda + \underline{f}_{\lambda\lambda} \Delta\lambda^2] \\ \omega &= -\mathbf{a}^T \underline{f}_\lambda \Delta\lambda - \frac{1}{2} \mathbf{a}^T [\underline{f}_{dd} \mathbf{a} \mathbf{a} \mu^2 + 2 \underline{f}_{d\lambda} \mathbf{a} \mu \Delta\lambda + \underline{f}_{\lambda\lambda} \Delta\lambda^2] \end{aligned} \quad (34)$$

With these manipulations it is thus possible to approximate (29) by a polynomial form of the type

$$g(\mu, \Delta\lambda) = A'_1 \Delta\lambda + 2A'_2 \Delta\lambda \mu + 3A''_2 \Delta\lambda^2 + 3A_3 \mu^2 + 6A'_3 \mu^2 \Delta\lambda + 4A_4^* \mu^3 + 6A'_4 \mu^3 \Delta\lambda + \dots \quad (35)$$

which is an expression that can be used to study all possible behaviors of the structure in the immediate neighborhood of the critical state x_c for small $\Delta\lambda$ and μ .

3.5. Basic results classical bifurcation theory

In elasticity, the cases that are most frequently encountered and that we will study here are governed by a shortened form of (35), i.e.

$$g(\mu, \Delta\lambda) = A'_1 \Delta\lambda + 2A'_2 \Delta\lambda \mu + 3A_3 \mu^2 + 4A_4^* \mu^3 \quad (36a)$$

where

$$\begin{aligned} A'_1 &= \mathbf{a}^T \underline{f}_\lambda; & A'_2 &= \frac{1}{2} [\mathbf{a}^T \underline{f}_{d\lambda} \mathbf{a} + \mathbf{a}^T \underline{f}_{dd} \mathbf{a} \mathbf{w}_{10}]; \\ A_3 &= \frac{1}{3!} \mathbf{a}^T \underline{f}_{dd} \mathbf{a} \mathbf{a}; & A_4^* &= \frac{1}{4!} \mathbf{a}^T \underline{f}_{ddd} \mathbf{a} \mathbf{a} \mathbf{a} - \frac{1}{2} \mathbf{w}_{02}^T \underline{f}_d \mathbf{w}_{02} \end{aligned} \quad (36b)$$

There are four types of behavior that can be identified on the basis of this classical result. They are given by

Limit point:

$$A'_1 < 0; \quad A_3 < 0 \quad (37a)$$

A-symmetric bifurcation point:

$$A'_1 = 0; \quad A'_2 < 0; \quad A_3 \neq 0 \quad (37b)$$

Symmetric bifurcation point (unstable):

$$\begin{aligned} A'_1 = 0; & \quad A'_2 < 0; \\ A_3 = 0; & \quad A_4^* < 0 \end{aligned} \quad (37c)$$

Symmetric bifurcation point (stable):

$$\begin{aligned} A'_1 = 0; & \quad A'_2 < 0; \\ A_3 = 0; & \quad A_4^* > 0 \end{aligned} \quad (37d)$$

The solutions that these conditions generate for very small values of $\Delta\lambda$ and μ are presented in Fig. 4

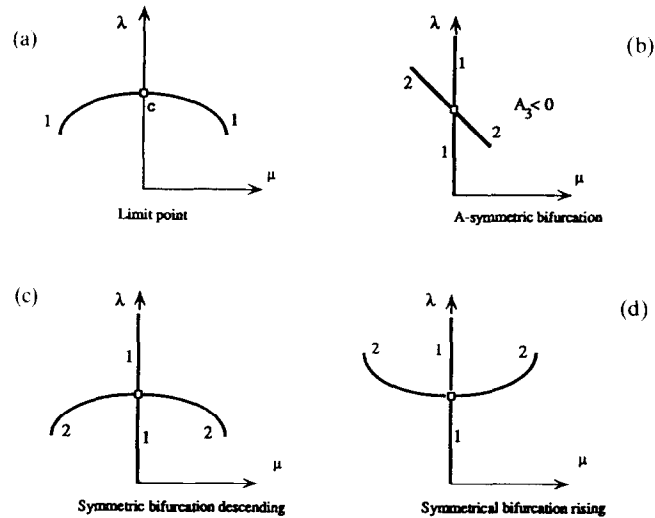


Fig. 4. The four elementary forms of loss of stability.

where the heavy lines denote the solutions of (36a) and the primary and secondary branches are labeled with the numerals 1 and 2.

The reader will have noticed that these results are derived exclusively on the basis of geometrical arguments. Whether these solutions are stable or not should still be verified. Such a task is relatively easy as long as we exclude the critical points from the solution branches pictured in Fig. 4. It can, for example, be carried out by an investigation into the condition of the Jacobian $\mathbf{K} = \mathbf{f}_d$, i.e. an investigation into the sign of the function $\Pi(\mu)$ defined by

$$\Pi = \text{MIN}_{\forall y \in R_N} \left\{ \frac{y^T \mathbf{f}_d(\Delta \mathbf{d}; \lambda_c + \Delta \lambda) y}{y^T y} \right\}$$

where

$$\Delta \mathbf{d} = \Delta \mathbf{d}(\mu); \quad \Delta \lambda = \Delta \lambda(\mu) \quad (38)$$

are the solutions of the branches defined by (29).

However, in this paper we will ignore this part of the analysis and focus on the question of the stability of the critical states themselves. This is an interesting problem, which, as it was shown by Koiter [8, 9] determines the basic features of the solutions presented by (37). As will be shown in the sequel, an analysis of this nature is not only useful for the characterization of the physical behavior of the solutions near and at the critical states, it will also provide clues that enable us to design a strategy that simplifies the solution of the mode jumping problem.

4. The notion of attraction and repulsion

4.1. The notion of stability

For ease of discussion (but without loss of generality) we introduce a shift in the origin of the configuration space choosing the equilibrium state under investigation as the center $\{\mathbf{d}; \lambda\} = \{\mathbf{0}; 0\}$. This means that we write for any perturbation from this state

$$\{\hat{\mathbf{d}}; \lambda\} = \{\mathbf{d} + \mathbf{y}; \lambda\} = \{\mathbf{y}; 0\} \quad (39)$$

Consequently, the equilibrium state under investigation is denoted by $\{\mathbf{0}; 0\}$, and it satisfies

$$f\langle \mathbf{0}; 0 \rangle = \mathbf{0} \quad (40)$$

As we are not interested in variations of the load for the moment, we write simply

$$f\langle \mathbf{0} \rangle = \mathbf{0} \quad (41)$$

Any perturbation from this state is now denoted by \mathbf{y} and this means that in general

$$f\langle \mathbf{y} \rangle \neq \mathbf{0} \quad (42)$$

Likewise, the potential energy measured from the center $\mathbf{y}=\mathbf{0}$ is written as

$$P = P\langle \mathbf{y} \rangle \quad (43)$$

We will now return to the general form of the energy criterion of stability. According to this criterion, stability of the equilibrium state $\mathbf{y}=\mathbf{0}$ is assured if we can find a neighborhood $\Omega_\varepsilon: \|\mathbf{y}\| < \varepsilon; \varepsilon > 0$ for which

$$P = P\langle \mathbf{y} \rangle > 0 \quad (44)$$

no matter how small ε is. In the case that this requirement is not satisfied, the equilibrium state $\mathbf{y}=\mathbf{0}$ is unstable [9].

We now intend to examine the character of this function in the neighborhood of $\mathbf{y}=\mathbf{0}$ in the special cases that we considered before, i.e. the limit point and the bifurcation points of Fig. 4. This examination is carried out in two steps. First we consider the conditions that determine the minimum of P around $\mathbf{y}=\mathbf{0}$ on a fixed distance $\|\mathbf{y}\|^2=r^2$ away from $\mathbf{y}=\mathbf{0}$. More specifically, introducing the Euclidean norm for $\|\mathbf{y}\|$ we look for the minimum of P on the sphere $\Omega\langle r \rangle$

$$\mathbf{y}^T \mathbf{y} - r^2 = 0 \quad (45)$$

where r =the radius of $\Omega\langle r \rangle$. After that we investigate under what conditions this minimum is positive for some interval: $0 < r < \varepsilon$.

The formulation of the minimum problem can be given in terms of the modified potential

$$P^\wedge = P\langle \mathbf{y} \rangle - \frac{1}{2} \kappa (\mathbf{y}^T \mathbf{y} - r^2) \quad (46)$$

where κ is the Lagrange multiplier that is needed to enforce the constraint (45). The stationary value of this function is given by the solution of

$$f\langle \mathbf{y} \rangle - \kappa \mathbf{y} = \mathbf{0} \quad (47a)$$

$$\mathbf{y}^T \mathbf{y} - r^2 = 0 \quad (47b)$$

If it is possible to find a solution $\mathbf{y}=\mathbf{y}_1$ of this problem that satisfies $P\langle \mathbf{y}_1 \rangle < P\langle \mathbf{y} \rangle$ for $\forall \mathbf{y} \neq \mathbf{y}_1; \mathbf{y}, \mathbf{y}_1 \in \Omega\langle r \rangle$ then the value of $P\langle \mathbf{y}_1 \rangle$ determines the minimum of $P\langle \mathbf{y} \rangle$ on $\Omega\langle r \rangle$. If $P\langle \mathbf{y}_1 \rangle > 0$, then also $P\langle \mathbf{y} \rangle > P\langle \mathbf{y}_1 \rangle > 0$ on $\Omega\langle r \rangle$. Stability of the configuration $\mathbf{y}=\mathbf{0}$ is assured when it is possible to find a bound, $\varepsilon > 0$, no matter how small, for which the function $P\langle \mathbf{y}_1 \rangle \langle r \rangle$ is positive and monotonically increasing in the range $0 < r < \varepsilon$.

4.2. Special paths that interconnect the equilibrium solutions in R_N

It is now noted that Eqs. (47) will possess many solutions, just as the equilibrium equations possess many solutions. Each one of these solutions represents a stationary value of the potential energy on the ball $\Omega\langle r \rangle$. If we vary the radius r , these solutions will also vary and in this way space curves $\mathbf{z}=\mathbf{z}\langle r \rangle$ are generated in R_N . In general, there are N space curves passing through $\mathbf{y}=\mathbf{0}$ as we will proceed to show. Note that the perturbation force $f\langle \mathbf{z} \rangle$ is always parallel to $\mathbf{z}\langle r \rangle$ (Eq. (47(a))).

A useful instrument in this consideration is the set of equations that determine the direction of the curves $\mathbf{z}\langle r \rangle$. For ease of discussion we replace the path parameter (r) by the arc length (s) of the curves

$\mathbf{z}\langle r \rangle$, so that we consider r as a function of s : $r = \rho\langle s \rangle$. If the path derivative in terms of (s) is denoted by $d/ds = (\cdot)'$, this change can be enforced by replacement of the subsidiary condition (47b) by

$$\int_0^s \mathbf{y}'\langle \sigma \rangle^T \mathbf{y}'\langle \sigma \rangle d\sigma - s = 0 \quad (48)$$

The equations of the (unit) tangent $\mathbf{z}\langle r \rangle'$ at $\mathbf{z}\langle r \rangle$ are then determined by

$$\begin{aligned} \mathbf{f}_d\langle \mathbf{z} \rangle \mathbf{z}' - \kappa \mathbf{z}' - \kappa' \mathbf{z} &= 0 \\ \mathbf{z}'^T \mathbf{z}' - 1 &= 0 \end{aligned} \quad (49)$$

Thus, for any curve \mathbf{z} passing through $\mathbf{y} = \mathbf{0}$, the equations that determine $\mathbf{z}'\langle \mathbf{0} \rangle$ are given by

$$\begin{aligned} \mathbf{f}_d\langle \mathbf{0} \rangle \mathbf{z}' - \kappa \mathbf{z}' &= 0 \\ \mathbf{z}'^T \mathbf{z}' - 1 &= 0 \end{aligned} \quad (50)$$

It can be seen that these equations determine the eigenvectors and eigenvalues of the Jacobian (or stiffness matrix) of the system (50) as well as that of Eq. (2) at \mathbf{d} . In general, the solution of the problem yields N eigenvectors \mathbf{z}'_i and N eigenvalues κ_i . We must thus conclude that there are N curves: $\mathbf{z}_i\langle s \rangle$ passing through $\mathbf{y} = \mathbf{0}$ (in general).

We now assume that the curves $\mathbf{z}_i\langle s \rangle$ that are studied here are smooth in the sense that they are differentiable as many times as we need. In that case, it must be possible to compute $\mathbf{z}_i\langle s \rangle$, at least in some neighborhood of $\mathbf{y} = \mathbf{0}$. It follows immediately from (49), that at the origin $\mathbf{y} = \mathbf{z}_i\langle s = 0 \rangle = \mathbf{0}$, the numerical values of the Lagrange multipliers $\kappa_i\langle 0 \rangle$ correspond to the eigenvalues of $\mathbf{K} = \mathbf{f}_d\langle \mathbf{0} \rangle$. When we move along the curves away from $\mathbf{y} = \mathbf{0}$, these values will change with s . Thus, the combination of \mathbf{z}_i and κ_i , the $N + 1$ dimensional vector $\mathbf{Z}_i\langle s \rangle = \{\mathbf{z}_i\langle s \rangle^T; \kappa_i\langle s \rangle\}^T$ also describes a curve in the space spanned by (\mathbf{y}, κ) .

There are at least two ways to interpret these space curves $\{\mathbf{z}_i\langle s \rangle; \kappa_i\langle s \rangle\}$. The first interpretation is that of special paths that are part of the energy surface and that reveal some of its global properties along the wave front $\mathbf{y}^T \mathbf{y} - r^2 = 0$ while: $r = 0 \rightarrow \infty$; i.e. they unveil some of the structure of the hills and the valleys of this surface.

The second way to interpret the paths $\mathbf{z}_i\langle s \rangle$ is to view them as a set of equilibrium paths, load deformation histories, that represent the response of the structure measured from $\{\mathbf{y} = \mathbf{0}; \lambda = 0\}$ when it is loaded by an additional and variable load equal to $\mathbf{b} = \kappa \mathbf{y}$ with κ as loading parameter. The original load $\lambda =$ is thereby kept constant. Note that from this point of view, the equations of equilibrium of the modified structure (47) can be written in the conventional form

$$\begin{aligned} \hat{\mathbf{f}}\langle \mathbf{y}; \kappa \rangle &= 0 \\ \mathbf{y}^T \mathbf{y} - r^2 &= 0 \end{aligned} \quad (51)$$

Just like any other equilibrium curve, the paths defined by (47) may possess bifurcation points and limit points (the latter defined with respect to κ). We note, however, that at points $r = r^*$ where $\kappa\langle r^* \rangle = 0$: $\mathbf{z}\langle r^* \rangle \neq \mathbf{0}$, we deal with solutions of (47) that coincide with that of system (2). In other words, when $\kappa\langle r \rangle = 0$ the solutions of (47) correspond to the equilibrium states of the original system. This means that each $\mathbf{z}_i\langle r \rangle$ can be viewed as a path in R_N that connects the center solution $\mathbf{y} = \mathbf{0}$ with other solutions \mathbf{y} of the equilibrium equations (Eq. (2)).

4.3. Reaction forces and the notion of attraction

What precisely is the meaning of the multiplier κ in Eq. (47)? It follows from (47) that it is possible to write

$$\mathbf{y}^T \hat{\mathbf{f}}\langle \mathbf{y} \rangle - \kappa \mathbf{y}^T \mathbf{y} = 0 \quad (52)$$

so that

$$\kappa = \frac{\mathbf{e}_y^T \mathbf{f}(\mathbf{y})}{r} = \frac{\mathbf{e}_y^T \mathbf{b}}{r}$$

where

$$\mathbf{e}_y = \frac{\mathbf{y}}{\|\mathbf{y}\|}$$

(53)

The Lagrangian constraint is thus proportional to the magnitude of the loading \mathbf{b} measured along the perturbation \mathbf{y} . This implies that the sign of κ determines whether the (external) loading \mathbf{b} is ‘pulling away’ or ‘pushing towards’ the center $\mathbf{y}=\mathbf{0}$. It is pulling when $\kappa>0$ and it is pushing when $\kappa<0$. Alternatively, if we look at the (internal) reaction force $\mathbf{f}(\mathbf{y})$, this force is ‘pulling back’ or ‘attractive’ when $\kappa>0$ and ‘pushing away’ or ‘repellent’ when $\kappa<0$. Thus, the reaction force tries to restore equilibrium when $\kappa>0$ but tries to destroy it when $\kappa<0$.

It can now be shown that the reaction forces $\mathbf{f}(\mathbf{y})$ are *always attractive* when the equilibrium state $\mathbf{y}=\mathbf{0}$ is stable. This follows from the observation that for any perturbation $\mathbf{y}=\mu\mathbf{n}$, where \mathbf{n} is an arbitrary unit vector.

$$\kappa = \frac{\mu\mathbf{n}^T \mathbf{f}(\mu\mathbf{n})}{\mu^2}$$

(54)

is always positive for $|\mu|$ small enough. To show this, we write for any arbitrarily small $\|\mathbf{y}\|=|\mu|>0$

$$\mathbf{f}(\mu\mathbf{n}) = \mathbf{f}(\mathbf{0}) + \mathbf{f}_d(\mathbf{0})\mu\mathbf{n} + A(\mu\mathbf{n})$$

(55)

where $A(\mu\mathbf{n})=\mu^2\mathbf{R}(\mathbf{n}; \mu)$ denotes the remainder of the expansion. Note that the *leading term* in $\mathbf{R}(\mathbf{n}; \mu)$ is of order 2 in \mathbf{n} and independent of μ . With (55) it can now be seen that

$$\kappa = \mathbf{n}^T \mathbf{f}_d(\mathbf{0})\mathbf{n} + \mu\mathbf{n}^T \mathbf{R}(\mathbf{n}; \mu) = \mathbf{n}^T \mathbf{f}_d(\mathbf{0})\mathbf{n} + \mu\mathbf{R}(\mathbf{n}; \mu)$$

(56)

and consequently

$$\kappa \geq \mathbf{n}^T \mathbf{f}_d(\mathbf{0})\mathbf{n} - |\mu|\|\mathbf{R}(\mathbf{n}; \mu)\| \geq \kappa_1 - |\mu|\|\mathbf{R}(\mathbf{n}; \mu)\|$$

(57)

The value κ_1 on the right-hand side of (57) is here the smallest eigenvalue of the problem (54). If the configuration $\mathbf{y}=\mathbf{0}$ is stable, we know that $\kappa_1>0$. This means that for the bound $|\mu|<\kappa_1/(\|\mathbf{R}(\mathbf{n}; \mu)\|)=\varepsilon>0$

$$\kappa = \frac{\mathbf{y}^T \mathbf{f}(\mathbf{y})}{\|\mathbf{y}\|^2} > 0$$

(58)

no matter in what direction the perturbation $\mathbf{y}=\mu\mathbf{n}$ points. Consequently, at a stable equilibrium state, the reaction forces $\mathbf{f}(\mathbf{y})$ are always forces of attraction as long as \mathbf{y} remains in $\Omega(\varepsilon): \mathbf{y}^T \mathbf{y} - \varepsilon^2 < 0$.

4.4. Perturbation forces at unstable states

If the configuration $\mathbf{y}=\mathbf{0}$ is unstable, there is at least one direction \mathbf{n} for which the reaction forces $\mathbf{f}(\mathbf{y})$ are repellent. This follows because in that case, the eigenvalue problem (50) has at least one solution for which $\kappa_1<0$. Let the associated eigenvector be denoted by \mathbf{a} ; $\|\mathbf{a}\|=1$. The value of $\bar{\kappa}$ in that direction is then

$$\bar{\kappa} = \frac{\mu\mathbf{a}^T \mathbf{f}(\mu\mathbf{a})}{\mu^2} = \mathbf{a}^T \mathbf{f}_d(\mathbf{0})\mathbf{a} + \mu\mathbf{a}^T \mathbf{R}(\mathbf{a}; \mu) = \kappa_1 + \mu\mathbf{R}(\mathbf{a}; \mu)$$

so that

(59)

$$\bar{\kappa} \leq \kappa_1 + |\mu|\|\mathbf{R}(\mathbf{a}; \mu)\|$$

This result shows that $\bar{\kappa}<0$ if μ is chosen small enough, i.e. the perturbation $\mathbf{y}=\mu\mathbf{a}$ induces a reaction

force that pulls the configuration \mathbf{y} away from the center $\mathbf{y}=\mathbf{0}$. This behavior is thus a clear indication of unstable behavior.

4.5. The perturbation forces at critical states

The previous results are not unexpected or surprising. Their significance is transparent and they already provide clues for the strategy that we need to develop for the initiation of the transient motion to be discussed later. However, to complete the picture that we started to paint, it is also desirable to investigate the qualitative behavior of the perturbation forces at the critical equilibrium states themselves. This task can be carried out directly by using Eqs. (47), but we prefer here to start the development from the very beginning, i.e. from the minimum problem (46). Again, we will restrict the considerations to the 4 particular cases of critical behavior discussed earlier.

In the same way as in Section 3, it is useful to introduce the decomposition

$$\mathbf{y} = \mu \mathbf{a} + \mathbf{v}; \quad \mathbf{a}^T \mathbf{v} = 0 \quad (60)$$

This leads to the modified potential

$$P^* = P\langle \mu \mathbf{a} + \mathbf{v} \rangle + \beta (\mathbf{a}^T \mathbf{v}) - \frac{1}{2} \kappa [(\mu \mathbf{a} + \mathbf{v})^T (\mu \mathbf{a} + \mathbf{v}) - r^2] \quad (61)$$

where β is the Lagrange multiplier that is needed to enforce the orthogonality condition in (60). Searching for the stationary value in the usual way leads to

$$\begin{aligned} \text{(i)} \quad \delta \mu: \quad & \mathbf{a}^T \mathbf{f} \langle \mu \mathbf{a} + \mathbf{v} \rangle - \mu \kappa = 0 \\ \text{(ii)} \quad \delta \mathbf{v} \quad & \mathbf{f} \langle \mu \mathbf{a} + \mathbf{v} \rangle + \beta \mathbf{a} - \kappa (\mu \mathbf{a} + \mathbf{v}) = 0 \\ \text{(iii)} \quad \delta \beta \quad & \mathbf{a}^T \mathbf{v} = 0 \\ \text{(iv)} \quad \delta \kappa \quad & (\mu \mathbf{a} + \mathbf{v})^T (\mu \mathbf{a} + \mathbf{v}) - r^2 = 0 \end{aligned} \quad (62)$$

Note that we made use of the property: $\mathbf{a}^T \mathbf{a} = 1$. We recall that in Eq. (62), (iv) is of little interest because it only defines the way we measure the length of the path that is described by the first three. Use of (i) in (ii) shows that we can eliminate β from (ii), because β must be equal to $\beta = 0$. Consequently, we are left with

$$\begin{aligned} \text{(i)} \quad & \mathbf{a}^T \mathbf{f} \langle \mu \mathbf{a} + \mathbf{v} \rangle - \mu \kappa = 0 \\ \text{(ii)} \quad & \mathbf{f} \langle \mu \mathbf{a} + \mathbf{v} \rangle - \kappa \mathbf{v} - \kappa \mu \mathbf{a} = 0 \\ \text{(iii)} \quad & \mathbf{a}^T \mathbf{v} = 0 \\ \text{(iv)} \quad & (\mu \mathbf{a} + \mathbf{v})^T (\mu \mathbf{a} + \mathbf{v}) - r^2 = 0 \end{aligned} \quad (63)$$

We will now seek the solution of these equations in an immediate neighborhood of the critical point \mathbf{d}_c defined by $\mathbf{y}_c = \mathbf{0}$ by solving (ii) + (iii) for $(\mathbf{v}, \kappa) = [\mathbf{V} \langle \mu \rangle, \mathbf{K} \langle \mu \rangle]$. As in Section 3, the decomposition (63) has the effect that the governing equations are split in a singular part (i) and a regular part (ii) + (iii). The latter part can therefore be linearized and solved locally around $\mathbf{y}_c = \mathbf{0}$. This will yield a solution for \mathbf{v} that we can use to evaluate the forces of the perturbation $\mu \mathbf{a} + \mathbf{v}$ along the path defined by (47) or (63).

It is useful to start the linearization of (ii) and (iii) by writing down the corresponding Newton form of these equations

$$\begin{aligned} & [\mathbf{f}_d \langle \mu \mathbf{a} + \mathbf{V} \rangle - \mathbf{K} \mathbf{I}] \Delta \mathbf{V} - [\mu \mathbf{a} + \mathbf{V}] \Delta \mathbf{K} = -\mathbf{r}(\mu \mathbf{a}, \mathbf{V}, \mathbf{K}) \\ & \mathbf{a}^T \Delta \mathbf{V} = 0 \end{aligned} \quad (64a)$$

where

$$\mathbf{r} = \mathbf{f} \langle \mu \mathbf{a} + \mathbf{v} \rangle - \mathbf{K} \mathbf{V} - \mathbf{K} \mu \mathbf{a} \quad (64b)$$

is the residual, V and K denote the initial estimates of v and κ , and ΔV and ΔK denote their corresponding corrections. The task is to find the solution of these equations in the neighborhood of $d_c = 0$ for a given, small value of μ .

The first guess for (V, K) can be given by

$$V = 0; \quad K = 0 \quad (65)$$

This leads to the corrector equations

$$\begin{aligned} f_d \langle \mu a \rangle \Delta V - \mu a \Delta K &= -f \langle \mu a \rangle = -\frac{1}{2} \underline{f_{dd}} a a \mu^2 + O(\mu^3) \\ a^T \Delta V &= 0 \end{aligned} \quad (66)$$

Note now that the Jacobian of this set

$$J = \begin{Bmatrix} K \langle \mu a \rangle & -a \\ a^T & 0 \end{Bmatrix} \quad (67)$$

is non-singular for small values of μ including $\mu = 0$. This shows that Eq. (63) is compatible for a certain range of μ .

A first approximation for the correction $(\Delta V, \Delta K)$ follows by neglecting μa in the argument of f_d and the terms of order $O(\mu^3)$ in the right-hand side of (66). The solution of Eq. (66) is then of the form

$$\Delta V = \mu^2 w_{02}; \quad \Delta K = \mu K_0 \quad (68)$$

With this result, we can write for κ along $\Delta d = \mu a + \mu^2 w_{02}$

$$\kappa = \frac{(\mu a^T + \mu^2 w_{02}^T) f \langle \mu a + \mu^2 w_{02} \rangle}{\mu^2 + \mu^4 \|w_{02}\|^2} \quad (69)$$

and a careful examination of the expansion of this expression reveals that the leading terms are given by

$$\kappa = 3A_3 \mu + 4A_4^* \mu^2 + O(\mu^3) \quad (70)$$

where

$$A_3 = \frac{1}{3!} a^T \underline{f_{dd}} a a; \quad A_4^* = \frac{1}{4!} a^T \underline{f_{ddd}} a a a - \frac{1}{2!} w_{02}^T \underline{f_d} w_{02}$$

The derivation is quite similar to that of the derivation of the reduced equation (36a) which explains why we do not feel the need to present it here.

It is now easy to see that the factor κ can be linked to the fundamental bifurcation equations (29), (36a) because κ can be written as

$$\kappa = \frac{1}{\mu} [3A_3 \mu^2 + 4A_4^* \mu^3 + O(\mu^4)] = \frac{1}{\mu} g \langle \mu, \Delta \lambda \rangle |_{\Delta \lambda = 0} \quad (71)$$

where $g \langle \mu, \Delta \lambda \rangle$ is given by (36). But the most interesting consequence of the result above is the possibility to sketch the nature of the forces that are induced by the perturbations $y = \mu a + \mu^2 w_{02}$ if these are applied at the critical states presented in Fig. 4.

It follows by inspection of (70) that the (reaction) force measured along y : $F = -\kappa \|y\| = -|\mu| \kappa$, has the following property

Limit point:

$$A_3 < 0 \rightarrow F = \text{attractive for } \mu < 0 \text{ and repellent for } \mu > 0 \quad (72a)$$

A-symmetric bifurcation point (unstable):

$$A_3 \neq 0 \rightarrow F = \text{attractive for } \mu < 0 \text{ and repellent for } \mu > 0 \text{ when } A_3 < 0. \text{ When } A_3 > 0 \text{ the situation is reversed.} \quad (72b)$$

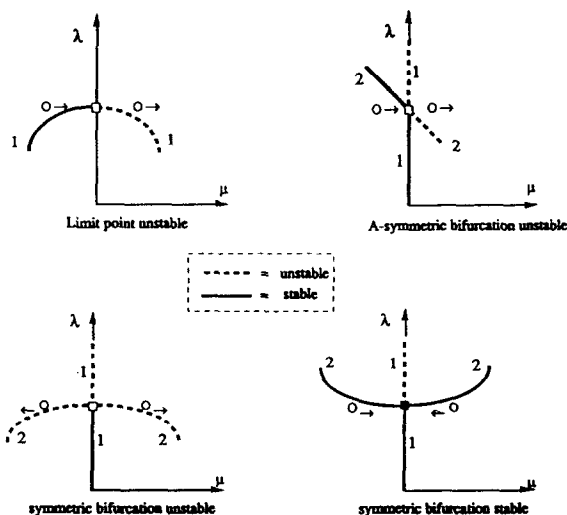


Fig. 5. Reaction forces in the μ direction at the critical loads.

Symmetric bifurcation point (unstable):

$$A_3 = 0; \quad A_4^* < 0 \quad \rightarrow F = \text{repellent, independent of the sign of } \mu. \quad (72c)$$

Symmetric bifurcation point (stable):

$$A_3 = 0; \quad A_4^* > 0 \quad \rightarrow F = \text{attractive, independent of the sign of } \mu. \quad (72d)$$

Fig. 5 gives an illustration of these reaction forces. It is of interest to note that these results completely agree with the investigations of Koiter who established that, for simple critical points, the qualitative character of the bifurcation branches, i.e. the postbuckling behavior, is determined by the stability properties of the critical states themselves [8, 9]. This observation implies for example, that the postbuckling branches are stable if and only if the bifurcation point itself is stable (and the other way around).

Koiter's investigation was also carried out on the basis of the energy criterion of Lagrange–Dirichlet but it dealt with the more difficult case of continuous systems [8, 9]. Our results, which are restricted to discrete systems, show that it is also possible to unfold this correspondence by addressing the question whether the critical state is (still) a proper attractor or not.

REMARK. It is not difficult to show that the critical points are still attractors if we restrain the motion in the direction of the eigenmode a .

5. The numerical procedure

5.1. The objective

We will now consider the actual computation of the response of a structural model under the influence of a quasi static loading process in a way that closely resembles the loading process in a testing machine, i.e. when the external loading is increased in a slow but steady fashion. In the beginning of such a process, when the state of deformation follows the stable part of the equilibrium path, the rate of change of the deformation of the actual structure is small, i.e. in correspondence to the rate of change of the load. But when the load reaches the value at which equilibrium becomes unstable, the behavior of the structure will change drastically. Small perturbations that are ever present will cause the structure

to escape the critical state and a motion occurs with a time rate of change of deformation that is orders of magnitude greater than it was seconds before. In view of this expectation, it seems natural to introduce some simplifications in the numerical simulation of this problem. Because $\dot{d} \approx 0$; $\ddot{d} \approx 0$ during the stable loading phase, it is possible to neglect these terms in (1) and approximate this part of the structures response by the static equilibrium path (2). On the other hand, when the jump occurs, the time interval Δt during which \dot{d} and \ddot{d} must be taken into account is very small. This means that during the transient phase of the response, the change in load can be neglected because $\Delta\lambda = \lambda' \Delta t \approx 0$.

The computation of the response curve of the structure can thus be carried out using a continuation method for the stable static part and a time integration method for the transient part. The only question that needs further consideration in this scenario is the way that the two methods must be matched. This is the topic of the following sections.

5.2. Computation of the quasi static part of the solution

We intend to compute the stable part of the solution path by a standard continuation method. The method that will be used is a predictor corrector procedure of a type that has been described at various places (see for example [13]). Here, it suffices to mention that the solution of the governing equations is obtained from the system of equations

$$\begin{aligned} f\langle \mathbf{x} \rangle &= 0 & \mathbf{x} \in R_{N+1}; & \quad f \in R_N \\ h\langle \mathbf{x} \rangle - \eta &= 0 & h \in R_1 \end{aligned} \quad (73)$$

where the extra equation is used to define the path parameter in the representation of the solutions

$$\mathbf{x} = \mathbf{x}\langle \eta \rangle; \quad \eta = \eta_1, \eta_2, \eta_3; \quad \text{etc.} \quad (74)$$

The predictor is either a linear or a quadratic extrapolation. The corrector process is of the type

$$A^i \Delta \sigma_k^i = -F\langle \sigma_k^i \rangle \quad (75a)$$

$$\sigma_k^{i+1} = \sigma_k^i + \Delta \sigma_k^i$$

$$A^i = F_x\langle \sigma_k^i \rangle \quad \text{or} \quad A^i = F_x\langle \sigma_k^0 \rangle \quad (75b)$$

where (k) is the step count for the solutions: $\mathbf{x}_k = \mathbf{x}(\eta_k)$, and (i) denotes the iteration count. The configuration σ_k^0 is the predicted solution for the step $\eta_{k-1} \rightarrow \eta_k$. Notice that this means that we apply Newton's method or the modified Newton's method. Because the corrector process produces a factored stiffness matrix, it is possible to solve the eigen problem

$$K\langle \mathbf{x}_k \rangle \mathbf{a}_k - \omega_k \mathbf{a}_k = 0 \quad (76)$$

at any converged state along the path and this means that it is always possible to obtain adequate information about the buckling mode of the critical point when such a point is approached.

The analysis begins with the computation of a series of points $\mathbf{x}(\eta_k)$ $k=1, 2, 3, 4, 5, \dots$ along the stable path for increasing values of the path parameter η . As long as the path is smooth, this task poses no difficulties. A slight complication arises, however, when it becomes necessary to pass a stable bifurcation point (Fig. 4(d)). In that case the path-following method must be guided along the stable path that branches off this point because that is the path the actual structure will follow when the load exceeds the bifurcation load.

The change of direction of the path-following method at a bifurcation point can be accomplished by several methods. The STAGS code [15], that we will be using here, has two standard options for such a switch. Method (a) is simply based on the determination of the direction of the branch 2 (see also Appendix A). Method (b) makes use of the Liapounov–Schmidt–Koiter reduction scheme to compute a new point $\mathbf{x}_2(\eta^* + \Delta\eta)$ on the branch 2. It will thus be assumed that we are able to follow the stable parts of the path even when they include stable bifurcations. In that case the need to interrupt these computations arises only at unstable critical states where change of stability occurs (from stable to

unstable). *Only* at these points does the actual structure suffer jumps and it is *only* at these points that we have to take special measures and enforce a change in the mode of operations.

5.3. Initialization of the transient phase of the computations

The critical points where jumping occurs are either limit points or unstable bifurcation points where change of stability occurs along the current branch. During the approach to these points the actual nature of the critical points is not known beforehand. This can only be determined after the critical point is detected and its approximate location has been computed. Identification of a limit point is the easiest. In that case, the path through the critical point is marked by a maximum in the λ vs. η diagram, with a change in the condition of the stiffness K .

If the singularity that is passed is a bifurcation point, it will generally be necessary to identify the type of point. There are two ways to carry this out. The first method is to design a perturbation expansion along the lines outlined in the previous section. The other consists of the determination of the bifurcation diagram in the immediate neighborhood of the bifurcation point using continuation and switch principles. We will consider the latter approach here, because like most codes for shell analysis, STAGS [15] does not possess capabilities for the determination of the bifurcation diagrams in terms of a perturbation expansion (at the present time).

It is comforting to realize that in the practical situation, bifurcation points are seldom encountered. This follows because it is often necessary to replace the pure bifurcation problem with an imperfect bifurcation problem. In fact, as will be discussed later, Stein's experiment can only be reproduced in a qualitatively acceptable manner if the model of Fig. 1 is slightly modified with imperfections. The effect of this perturbation is that the bifurcations disappear. In other words, the imperfect structures approach does not only lead to a much easier treatment of the jumps, it also results in a more realistic response of the structure. But, for the time being, we will consider the encounter with bifurcation points as a realistic possibility in the discussion that now follows.

Suppose the calculations that have been carried out in the static domain have produced a certain set of discrete points around the critical state. Suppose further that from this calculation the unstable character of this state has been established. At that moment, the solution procedure should be switched to the solution of the equation of motion

$$M\ddot{\mathbf{d}} + D\dot{\mathbf{d}} + \mathbf{f}(\mathbf{d}; \lambda) = 0 \quad (77)$$

It is clear that this integration process must be started with appropriate initial conditions

$$\mathbf{d}(0) = \mathbf{d}^*; \quad \dot{\mathbf{d}}(0) = \dot{\mathbf{d}}^*; \quad \lambda = \lambda^* \quad (78)$$

because the ensuing motion should correspond to the expected jump phenomenon, i.e. to the response that is likely to occur in practice.

As mentioned in the Introduction, for the actual structure in the testing machine, this question of initiation is not important because the structure is subjected to fluctuating perturbations from \mathbf{d}_c that eventually will lead to the jump motion. For the numerical simulation, the situation is different because (78) is then applied in a unique way, i.e. every particular choice will result in a particular motion, but not every choice will also trigger the jump. Consequently, the question needs to be addressed whether there is a guideline by which these conditions can be formulated. Note that the initialization (78) concerns a static and a temporal part. We first discuss the static part by assuming that $\dot{\mathbf{d}}(0) = \mathbf{0}$.

The considerations of Section 4 suggest that, in order to escape from an unstable critical state \mathbf{d}_c , we should use the initial conditions (78) with the value: $\mathbf{d}^* = \mathbf{d}_c + \mu \mathbf{a} + \mu^2 \mathbf{w}_{02}$. The shift $\mu \neq 0$ must then have the sign that corresponds to the 'escape' direction (see Fig. 5) because this particular perturbation then guarantees the initiation of a motion away from \mathbf{d}_c . Indeed, there is no doubt that this proposition will lead to the intended effect, but it suffers from the drawback that it requires the computation of the second-order perturbation term $\mu^2 \mathbf{w}$. This is a term that is usually not (immediately) available during the type of computations that are discussed here. Therefore, it turns out to be more practical to

introduce a modification that does not rely on the second order term, but on an additional shift with respect to the load

$$\mathbf{d}^* = \mathbf{d}_c + \mu \mathbf{a}; \quad \lambda^* = \lambda_c + \Delta\lambda; \quad \dot{\mathbf{d}}^* = 0 \tag{79}$$

$$\text{for } |\mu| > 0; \quad \Delta\lambda > 0$$

where μ must have the appropriate sign (only relevant in the case of an a-symmetrical bifurcation point).

As it can easily be verified, these conditions will guarantee a ‘push’ in the ‘escape’ direction \mathbf{a} , in part through the effect of the increase of the load from λ_c to $\lambda_c + \Delta\lambda$. Illustrations of the qualitative effect of this measure are given in Fig. 6. The forces shown in this figure are the reaction forces in response to a perturbation of the type (79), with $|\mu|, |\Delta\lambda|$ chosen ‘arbitrarily small’.

With these observations we are now able to define the following practical measures that will initiate the transient motion from the critical states. The continuation procedure should be applied until the suspected critical state is passed so that a point of the primary path is computed that we denote by $\mathbf{x}_1(s_c + \Delta s)$. At that moment, the computations should be switched to the transient procedure with initial conditions

$$\mathbf{d}^* = \mathbf{d}_1(s_c + \Delta s) + \mu \mathbf{a}; \quad \lambda^* = \lambda_1(s_c + \Delta s) + \Delta\lambda; \quad \dot{\mathbf{d}}^* = 0 \tag{80}$$

where $\Delta s, \Delta\lambda$ and $|\mu|$ are small positive increments that must be properly chosen.

5.4. Particular cases

Initialization of the transient motion from a limit point on the basis of (80) turns out to be particularly simple. This follows because any state beyond the limit point

$$\mathbf{x}(s_c + \Delta s) = \left\{ \begin{matrix} \mathbf{d}(s_c + \Delta s) \\ \lambda(s_c + \Delta s) \end{matrix} \right\} \quad \text{for small } \Delta s > 0 \tag{81}$$

already contains a measure of the mode \mathbf{a} (see Section 3.2 and Appendix A). All that needs to be done is to raise the load factor $\lambda(s_c + \Delta s)$ by an (positive) amount at this state so that one should apply

$$\begin{aligned} \mathbf{d}^* &= \mathbf{d}(s_c + \Delta s); & \dot{\mathbf{d}}^* &= 0 \\ \lambda^* &= \lambda(s_c + \Delta s) + \Delta\lambda > \lambda_c \end{aligned} \tag{82}$$

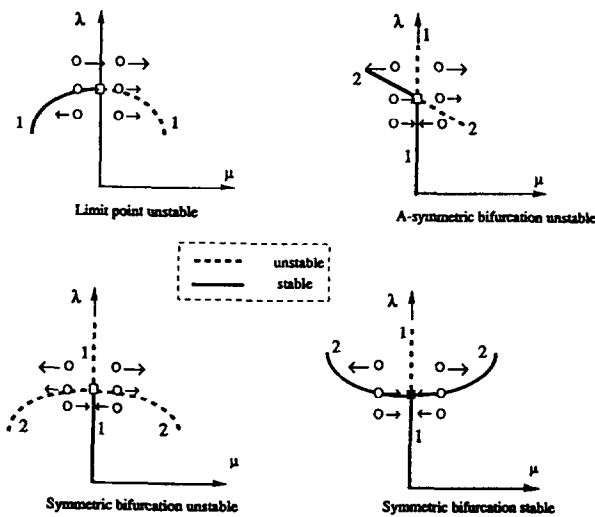


Fig. 6. Reactive forces for perturbations in the λ - μ plane.

It is further noted that at *non*-symmetrical bifurcation points, it is not possible to decide what sign μ must have without computing the coefficient $A_3 = (1/3!) \mathbf{a}^T \underline{f}_{\mathbf{a}\mathbf{a}} \mathbf{a}$. If A_3 can be computed, the prescription is

$$\text{Sign}(\Delta\mu) = -\text{Sign}(A_3) \quad (83)$$

If this information is not available, one can use the method of trial and error.

It is finally noted that in the remaining two cases, the symmetrical bifurcation points with $A_4^* < 0$ or $A_4^* > 0$, no amendments are necessary. If the bifurcation point is unstable, the transient procedure will compute a trajectory that eventually will reach an end point that belongs to a stable equilibrium path not necessarily connected with the bifurcation point. On the other hand, if the bifurcation point is stable, the trajectory is expected to end at a point of the rising branch 2 of the bifurcation point. In this special case, *the mode jump technique takes the role of a switch technique for the static path-following procedure* that makes it possible to continue the computations along the stable branch of the bifurcation point. Note that, in general, the jump technique can be seen as a switch technique that connects stable parts of the solution set of (2).

5.5. The use of initial velocities

So far we discussed only the initialization of the transient motion for the case that $\dot{\mathbf{d}}^* = 0$. This special class of choices seems to be the best possible in cases where one tries to simulate buckling experiments in the laboratory under dead weight or prescribed end-shortening loading conditions. As was already indicated, in these situations the load is increased very slowly with time and it is then not to be expected that the dynamic snap when the limit load is reached will be initiated by an initial velocity field $\dot{\mathbf{d}}^* \neq 0$.

A different situation arises when one wants to expedite the computation of the transient motion and is not so much interested in the authenticity of the animation. In that case, the temporal part of the initialization (78) allows us to give the structure an initial velocity by which the jumping process can be accelerated. It goes almost without saying that an initial velocity in the escape direction \mathbf{a} , thus $\dot{\mathbf{d}}^* = \varepsilon \mathbf{a}$, where ε is some positive or negative number, should here be the proper selection.

REMARK. Perhaps there is a danger connected with this approach. The modification of the initial conditions for the jump effects changes in the transient motion. The resulting orbit will differ from that which is calculated with $\dot{\mathbf{d}}^* = 0$ and it is not certain that the endpoint will be the same. The addition of an initial velocity is thus only useful in cases where the resemblance of the simulation with the test is not of great concern (see also the discussion about the uniqueness of the jump process at the end of this paper).

5.6. Initialization of the quasi static solution phase

The computation of the transient motion can be carried out by any procedure that is available. In the STAGS program, we used Park's method [15, 16]. This is an implicit method with very robust characteristics. For a description of the method refer to [16].

The points along the transient path that are obtained starting from the jump conditions (80) will eventually approach a new point of attraction, a stable equilibrium state $\mathbf{x}_2^* = \{\mathbf{d}_2^T; \lambda_c + \Delta\lambda\}^T$. This will happen when the dynamic state of the structure cannot escape the forces of attraction of \mathbf{d}_2 , starts orbiting \mathbf{d}_2 and eventually, due to the dissipation of energy, closes in to \mathbf{d}_2 . The damping introduced in our model is the mechanism behind this energy dissipation during the motion between \mathbf{d}_1 and the new stable state \mathbf{d}_2 . According to the equations of motion, the integral

$$\int_0^t \dot{\mathbf{d}}^T(\tau) \{ \mathbf{M} \ddot{\mathbf{d}}(\tau) + \mathbf{D} \dot{\mathbf{d}}(\tau) + \mathbf{f}(\mathbf{d}(\tau); \lambda) \} d\tau = 0 \quad (84)$$

represents the balance of energy during the jump. The three integrals concern the kinetic energy the T_2 , dissipated energy Q_2 due to damping and the drop in potential energy ΔP . It is thus possible to write

$$T_2 = \int_0^t \dot{\mathbf{d}}^T \langle \tau \rangle \mathbf{M} \ddot{\mathbf{d}} \langle \tau \rangle d\tau; \quad Q_2 = \int_0^t \dot{\mathbf{d}}^T \langle \tau \rangle \mathbf{D} \dot{\mathbf{d}} \langle \tau \rangle d\tau; \quad \Delta P = \int_0^t \dot{\mathbf{d}}^T \langle \tau \rangle \mathbf{f} \langle \mathbf{d} \langle \tau \rangle; \lambda \rangle d\tau \quad (85a)$$

$$T_2 \langle t \rangle + Q_2 \langle t \rangle + \Delta P \langle t \rangle = 0 \quad (85b)$$

It follows that when $t \rightarrow \infty$; $T_2 \rightarrow 0$. The damping matrix is chosen to be positive definite and this means that the drop of the potential energy $\Delta P = P \langle 2 \rangle - P \langle 1 \rangle$ associated with the difference between the potential energy at \mathbf{x}_{1c} and \mathbf{x}_2^* will eventually be absorbed in Q_2 so that $Q_2 \langle \infty \rangle = -\Delta P \langle \infty \rangle$.

It is this observation that guides us during the numerical simulation of the jump. During the calculations, the kinetic energy will ultimately, i.e. after a time t_r , satisfy

$$T_2 \langle t \rangle < \varepsilon_T \quad \text{for } t > t_r \quad (86)$$

where ε_T is a small positive number. The small value of the kinetic energy is then an indication that a new stable state is nearby. This means that we will assume that configurations $\xi = {}^1\mathbf{x} \langle t > t_r \rangle$ for which 7(86) holds, are close to ${}^1\mathbf{x} \langle \infty \rangle$, see also Section 2.

When (86) is ascertained, i.e. when a configuration $\xi = {}^1\mathbf{x} \langle t = t_1 > t_r \rangle$ is expected to be close to a static equilibrium state $\psi = \mathbf{x}_2^*$, it can be used as predictor in Newton's method to obtain ψ . With this approach, convergence is guaranteed if (i) $\mathbf{K}(\psi)$ = definite and (ii) the predictor ξ is in the domain of convergence around ψ . Because the satisfaction of these conditions can never be known beforehand, it is possible that this process fails and that it is necessary to continue the transient analysis until a configuration $\xi = {}^1\mathbf{x} \langle t_2 > t_1 \rangle$ is reached from where the initiation process just described can be restarted. In this connection, any other suitable correction process can be used in order to obtain ψ . For example, the STAGS code is equipped with a relaxation method that defines a smooth path $\Xi(\eta)$ between ξ and ψ , and that computes this path from ξ to ψ by a path-following method. This procedure is more complicated but also more robust than the simple Newton iteration described earlier. It can be used when attempts with the other method fail.³

If the computation of ψ is successful, the calculations can be continued by computing the path $\mathbf{x}_2(s)$ that goes through ψ . The direction along $\mathbf{x}_2(s)$ that one takes is dependent on the purpose of the analysis. In this paper this direction always corresponded to an increasing load λ . It is noted in passing that, during the switch from the dynamic mode to the static mode, the stability of the new state ψ can be ascertained by monitoring the condition of the Jacobian $\mathbf{K}(\sigma^i)$ where σ^i denotes the iterates that approach ψ . For ψ to be stable $\mathbf{K}(\psi)$ should, of course, be positive definite.

6. Examples and conclusion

6.1. M. Stein's example

The buckling tests of M. Stein were already described in the Introduction. A sophisticated analytical study of a model of this experiment was given in [6, 7]. The model consists of a plate strip that is simply supported along the longitudinal edges and clamped along the loaded edges. The panel aspect ratio: l/b of the experiment was 5.38. But in the analysis [6, 7] it was taken as: $l/b = 5.92$ to induce the coincidence of two buckling modes at the critical value of the load λ_c . The authors used a Liapounov-Schmidt reduction technique to analyze the nature of the branching behavior of this model configuration. They discovered that the branch corresponding to the mode with 5 half waves is rising but unstable for a small increase of the load, while the branch characterized by 6 half waves is stable. From this result it is possible to explain why the actual panel changes its mode shape by jumping away from the unstable branch 5 to the stable branch with 6 half waves.

In the calculations that are presented here, the original dimensions $l/b = 5.38$ of the panel are retained because the numerical simulation is aimed at a repeat of the behavior as observed in the

³ In our experience, the simple Newton iteration from ξ to ψ was always successful when T_2 was 'small enough'.

experiment. It is also important to keep in mind that a distinction is made between a *perfect panel* as defined by the data of the experiment and *imperfect panels*. In the latter cases, the perfect plate strip geometry is slightly changed by adding displacement patterns in terms of combinations of the buckling modes that were previously calculated from a linear buckling analysis.

6.1.1. Model definition

Just as in [7], the model that we introduced for the buckling simulation is confined to a plate strip of width b , assuming simple support at $y = -1/2b$, $y = 1/2b$. These are boundary conditions that approximate the knife edge supports that were applied at $y = (k - 1/2)b$ ($k = 1, 2, \dots, 6$) in the test. We refer to Fig. 7 for the basic conventions as regards to the choice of the reference frame and definition of the displacement components u, v, w that represent the displacement of the mid-plane of the plate. Note that the rotations around the axis x, y, z are denoted by $\beta_x, \beta_y, \beta_z$.

Because the deformation across the plate strip model is expected to be symmetrical to the plane $y = 0$, the finite element model could be confined to one half of the strip as is indicated in the figure by the plate strip half with edges labeled 1, 2, 3, 4. The boundary conditions that we applied on this part of the plate can be described as follows:

1. A special clamping condition: $u = 0, v = \text{free}, w = 0, \beta_x = 0, \beta_y = 0, \beta_z = 0$
2. Simple support: $u = \text{free}, v = \text{constant}, w = 0, \beta_x = \text{free}, \beta_y = 0, \beta_z = 0$
3. A special clamping condition: $u = \text{constant}, v = \text{free}, w = 0, \beta_x = 0, \beta_y = 0, \beta_z = 0$
4. Symmetry: $u = \text{free}, v = 0, w = \text{free}, \beta_x = 0, \beta_y = \text{free}, \beta_z = 0$

The loading is introduced at edge 3. As follows from the formulation above, the edge can move uniformly in the x -direction. On this rigid edge the load λF_0 is applied. The reader will observe that we allowed the plate to adopt a uni-axial state of stress in the pre-buckling state of the perfect plate by omitting the suppression of the tangential displacement v at boundary 1, 2, 3. This choice is not in complete agreement with the conditions in the actual test but it is a choice that is acceptable within the context of the other assumptions made. The shell elements used (code 410 in the STAGS manual) represent a small strain, but arbitrarily large rotation and displacement theory [15]. The physical properties that we introduced are:

Isotropic plate material, Young's modulus $E = 70\,000 \text{ N/mm}^2$; Poisson's ratio $\nu = 0.3$, mass density = 2.79 kg/m^3 . For the damping we used the relation

$$D = \alpha M + \beta K \quad (87)$$

The coefficients α and β were based on a vibration analysis that was conducted on the plate. When the dominant frequency of the plate during the transient phase of the response is given by ν , a natural choice for the damping (87) of the plate will be

$$\alpha = 2\pi\nu\kappa \quad (88)$$

$$\beta = \frac{\kappa}{2\pi\nu}$$

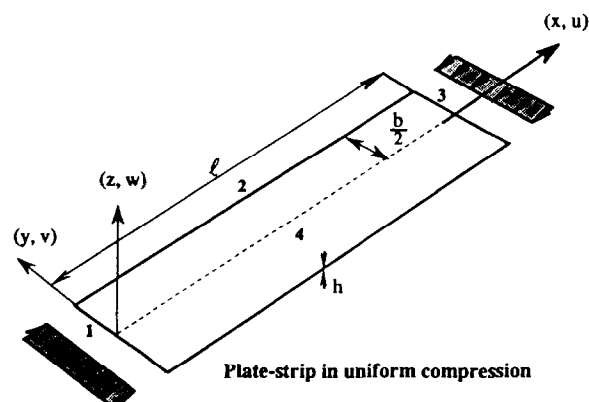


Fig. 7. Model definition.

where κ is a number <1 , for example between 0.05 and 0.2. A rough estimate of the dominant frequency is the lowest non-zero eigenfrequency of the plate, either under load or without a load. With this approach we can introduce a measure of damping that is under the critical value. In the case of the plate, the values for α , and β set in this way were: $\alpha = 80$; $\beta = 0.125E - 3$.

6.1.2. Preliminary considerations

The linear buckling analysis of the perfect panel revealed that the first mode, with five half waves along the length of the panel, Fig. 8(a), appears at $\lambda_c = 1$. The second, with 6 half waves at $\lambda_2 = 1.006$, the third with 6⁴ half waves at $\lambda_3 = 1.09$, etc. Consequently, we are dealing with eigenvalues that are very close.

But in spite of the closeness of the eigenvalues, the first bifurcation point at the value $\lambda_c = 1$ turns out to be a simple bifurcation point. According to our knowledge of plate buckling phenomena, it is to be expected that this point is stable so that for a load slightly in excess of the critical value λ_c the structure will still be able to carry load. The bifurcation point is symmetric, and is of the pitchfork type, see Fig. 4(d). A classical analysis such as given in [7] would bear this out immediately. However, how the branching diagram looks like for values of λ further removed from the critical value is very difficult to uncover, not only with classical analytical methods but also with path-following methods. This difficulty is related to the circumstance that in a relatively small region around the critical state x_c the branching solutions for λ_c , λ_2 , λ_3 , etc. are intertwined, with several secondary bifurcations representing the interactions that occur along these solutions between the various buckling modes.

6.1.3. Imperfect panel

The load deformation response of the perfect model can be calculated following the procedure outlined in Section 5. However, this response does not produce the 5 to 6 half wave mode jump that was observed in the experiment. This happens to be so because the static and transient solutions of the plate will stay in the space that is defined by modes that are symmetrical with respect to the mid-plane $x = 1/2l$. In other words, the perfect model jumps from 5 to 7 and from 7 to 9, etc. However, the test article from which the numerical model is derived was not perfect. Although the imperfections were not measured, it is clear that they must have destroyed the symmetry that was initially designed into the plate. Clearly, the authenticity of the simulation can be enhanced by adding geometrical imperfections to the plate so that the symmetry of the plate configuration is broken. From a numerical point of view, this modification has the advantage that it promotes mode jumping to occur from limit points rather than bifurcation points and therefore it promotes an easier control of the flow of calculations.

Consequently, we added a combination of the first three buckling modes as initial imperfections to break the symmetry of the plate configuration.

If the first three modes (see Fig. 8) are denoted by \mathbf{a}_1 , \mathbf{a}_2 , \mathbf{a}_3 , the imperfections introduced are given by

$$\mathbf{w}_0 = 0.1[\mathbf{a}\langle 1 \rangle + \mathbf{a}\langle 2 \rangle + \mathbf{a}\langle 3 \rangle]h \quad (89)$$

where h = the thickness of the plate and the modes $\mathbf{a}\langle i \rangle$ are normalized as

$$\|\mathbf{a}\langle 1 \rangle\| = 1 \quad \text{where } \|\mathbf{a}\langle i \rangle\| = \text{MAX} \{|\mathbf{a}\langle i \rangle \mathbf{e}_k|\}_{k=1,2,3..} \quad (90)$$

6.1.4. Results of the calculations

The response calculation began with the initial stable response curve of the problem. This revealed that the plate reaches the first critical equilibrium state at a limit point at $\lambda_{c5} = 1.5$. At this point the deformed shape of the plate is dominated by 5 half waves and we denote the branch of solutions that go through it X_5^* . At the limit point we started the mode jump procedure in the manner described in Section 5. The jump resulted in a change from 5 to 6 half waves so that a branch denoted by X_6^* was

⁴ Mode 3 has 6 halfwaves, two of which are very small (at the center of the plate). The existence of these waves were confirmed by two independent checks with other computer codes.

(a)

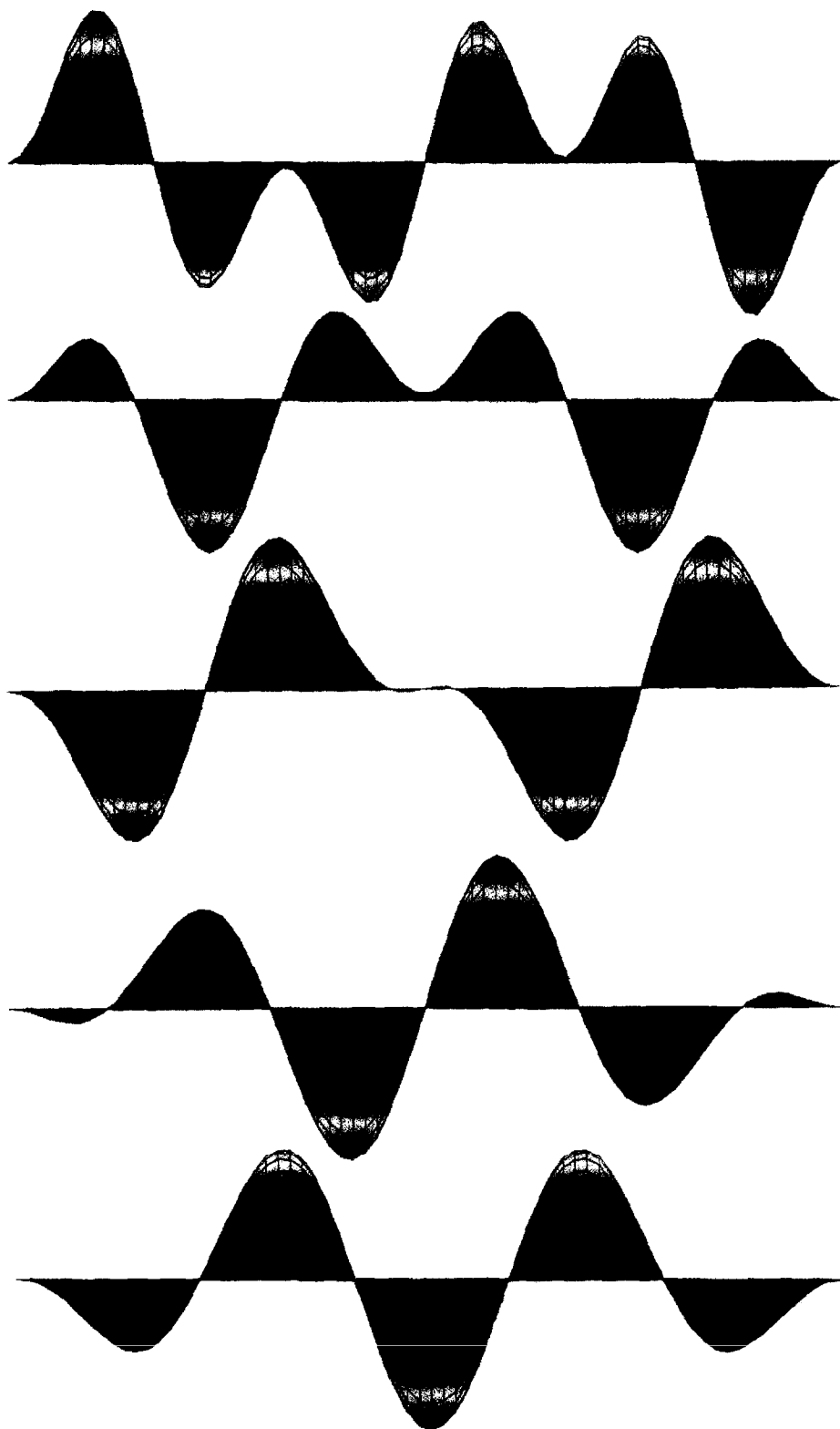


Fig. 8. (a) Buckling modes.

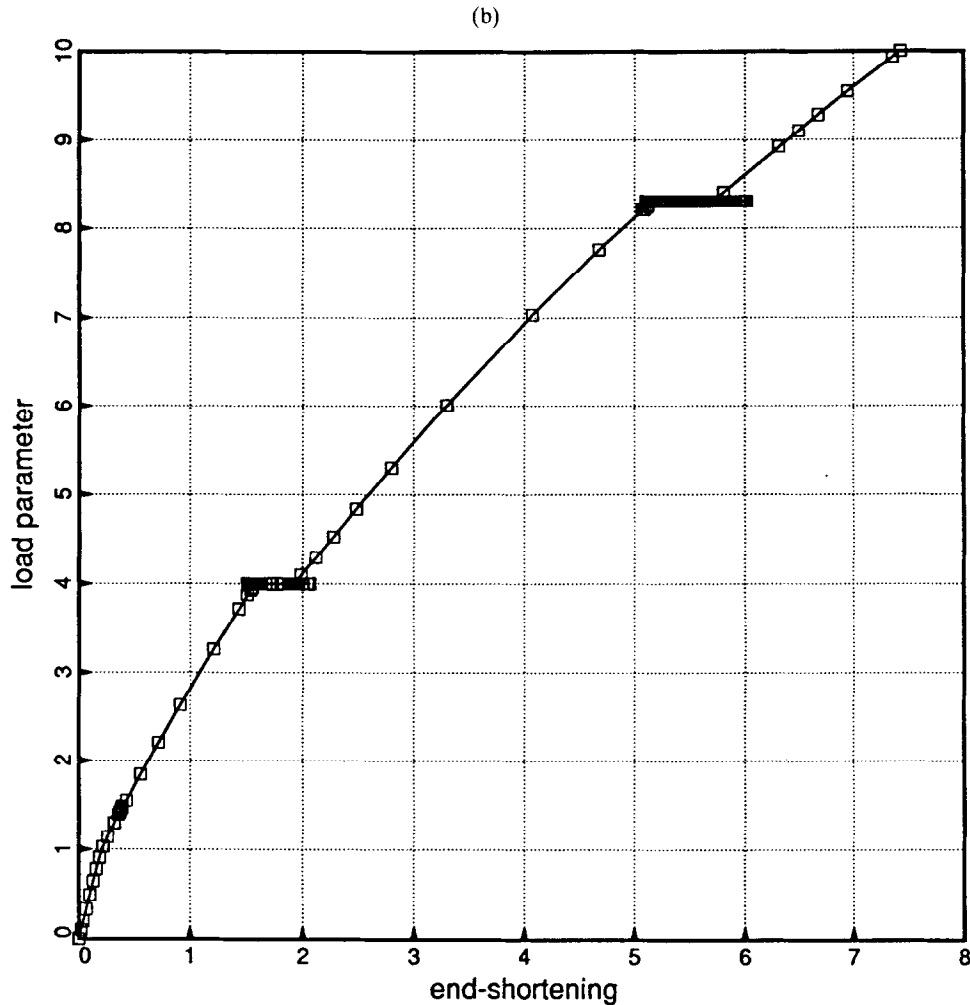


Fig. 8 (b) Response of the plate.

reached. After the switch to the static procedure the branch X_6^* was traversed until a second limit point was reached at $\lambda = \lambda_{c6} = 4.0$. From this point we performed a second modejump run and the result was a change of the mode shape from 6 to 7 at X_7^* . Continuing in this manner we were able to compute jumps from 7 to 8 and from 8 to 9 and so on. Of course, in the actual experiment, the jumps from 7 to 8, etc. were taking place in the plastic range, but that is not of any concern here.

The summary of these results is given in Fig. 8(b) in the form of a load vs. end-shortening diagram (only the jumps from 5 to 6, from 6 to 7 and 7 to 8 are shown here). It can be concluded that our computations show a series of mode jumps that are qualitatively similar to those observed by M. Stein. The remaining differences that exist between his test results and the numerical results must be based on the observation that the actual behavior of the structure is always very sensitive to perturbations in the data that define the buckling problem, i.e. the boundary conditions, the imperfections and the material properties.

6.2. The buckling simulation of a cylindrical shell in compression

A second example of the potential of the hybrid solution strategy is the simulation of the behavior of a thin-walled cylindrical shell in compression. The buckling experiment that we took as an example was

recently carried out at NASA and a description of the test can be found in [17]. Here, it suffices to give a short summary of the numerical simulation of this test.

6.2.1. *The model*

The test article consisted of a graphite-epoxy composite cylindrical shell of 7.976 in. radius and a 0.040 in. wall thickness. The wall is made of a 8 ply quasi-isotropic laminate with a stacking sequence of $[+45/0/90]^5$. It was tested in the testing machine by applying axial compression with controlled end-shortening. For readers who are not familiar with these tests we should add the following note: As compared to load control (=dead loading [9–11]), controlled end-shortening loading leaves the shell intact after buckling has taken place. The difference in behavior between these two alternative ways of testing is related to the circumstance that under end-shortening control, there is only membrane energy available for conversion into bending energy during the buckling process, while in the case of dead weight control, there is also a substantial amount of (extra) potential energy available. For additional details refer to Rankin et al. [17].

A most important feature of the test article is that the geometrical imperfections were carefully measured. In the STAGS model we used a Fourier representation of these measurements consisting of a 24×90 terms series that approximates the measured imperfections with a small error [17]. The discretization that was used for this model produced 34347 computational degrees of freedom. The bandwidth of the stiffness matrix was 638.

6.2.2. *Results*

The standard continuation procedure needed five load steps to reach the limit point. After this point was passed in step 7 we applied the initial (limit point type) conditions described in Section 5, to initiate the transient part of the solution. During the transient phase of the response the cylinder experienced a considerable change in the wave pattern over the surface. This can be seen in Fig. 9(a–d). The last picture, Fig. 9(d), represents the deformation state of the cylinder in the stable postbuckling state. Notice the way the waves start and spread around the circumference as can be seen by comparing Fig. 9(a–d) with Fig. 9(e,f). Fig. 10 shows the complete load end-shortening history of the simulation while the kinetic energy vs. time history of the buckling process is given in Fig. 11.

It is noted that the stable postbuckling state that is reached at the end of the transient phase is maintained at a considerable drop in the compressive load: 45%, see Fig. 10.

The interesting feature of the visual part of this deformation mode is that it *does correspond* with the postbuckling shape observed in the experiment. But, as far as the critical load value λ_c is concerned, our simulation overestimates the registered buckling load by a factor of 23%.

The reason for the discrepancy is not difficult to understand. The shell is imperfection sensitive not only with respect to changes in the geometry, but also with respect to the application of the load (eccentricity) and the integrity of the laminate buildup. It should further be mentioned that any attempt to reach the far post buckling state by path-following alone failed. This failure is due to the degenerate character of the solution path beyond the limit point (the unstable path is riddled with bifurcations), and these singularities cause the path-following method to break down.

REMARK. Even if the difficulty last mentioned does not exist, there still is no guarantee that the continuation procedure will reach the stable post buckling state that is pictured in Fig. 9(d). This follows, because it is not certain that the fundamental path 1 is connected with this particular post buckling state.

6.3. *Discussion*

The two examples presented in this paper show very clearly that it is relatively easy to combine continuation and transient analysis capabilities into one tool which is able to compute the entire buckling process of a shell. A word of caution is necessary, however. There is no evidence that the jumps to far field stable states are unique. By this we mean that it is quite possible that, for different initial conditions and different choices of damping, other post buckling states will be reached.

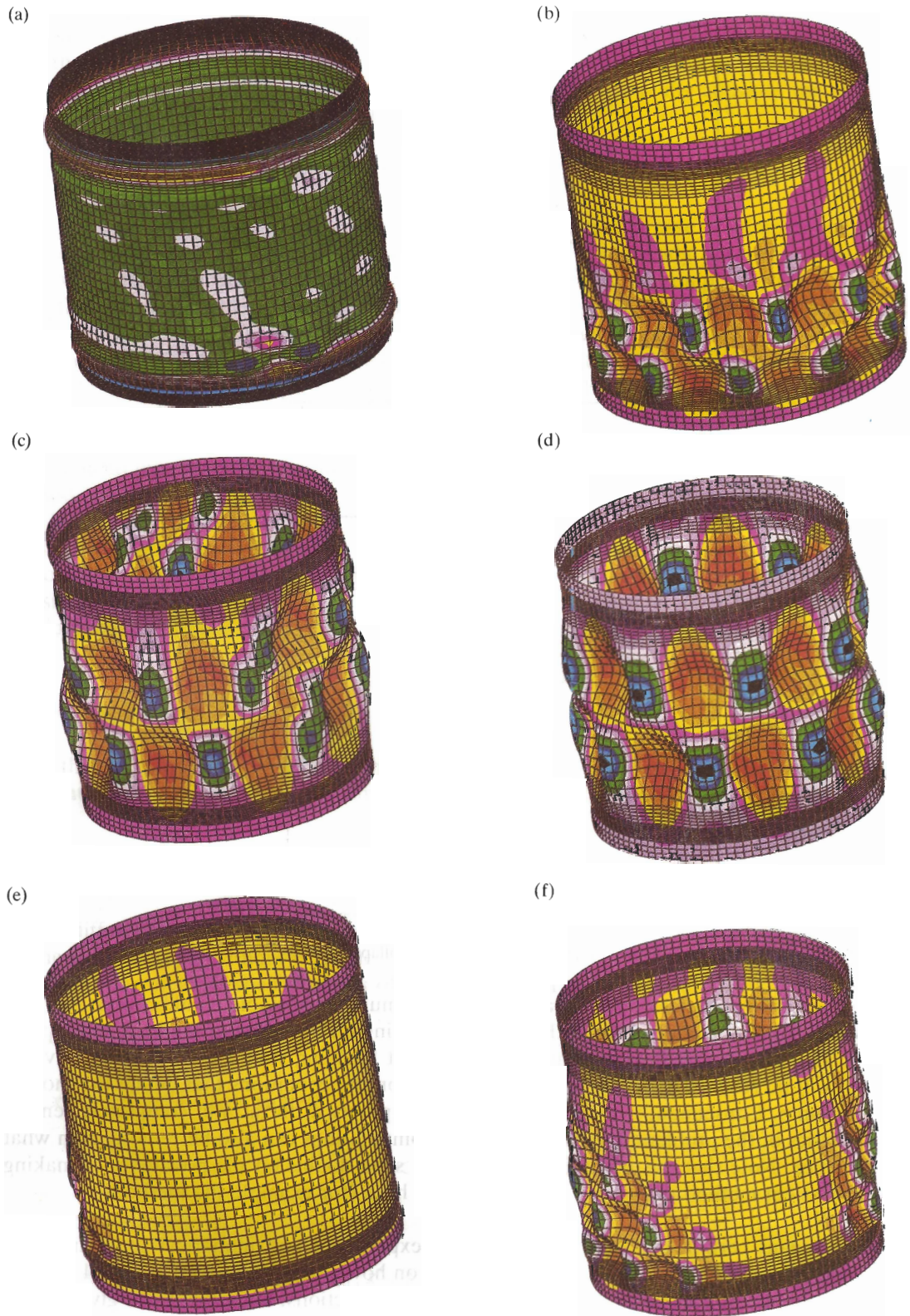


Fig. 9. (a–d) Snapshots of the buckling motion (a: loadstep 7, just before collapse; b: step 160; c: step 285; d: step 384); (e,f) some alternative takes ((e: step 160; f: step 245).

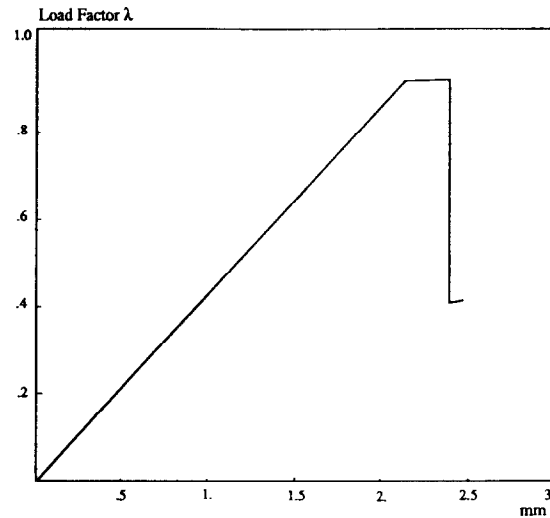


Fig. 10. End-shortening vs. load.

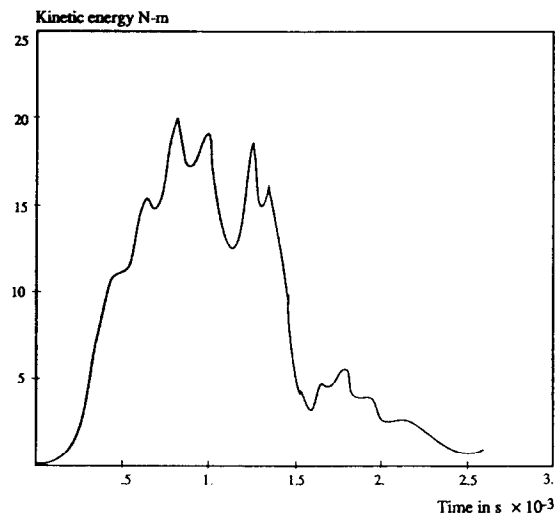


Fig. 11. Kinetic energy history during the collapse process.

It is known from extensive studies on spherical caps, that the number of stable equilibrium states that exist for thin shells is small, but is often more than one (depending on the value of the load and type of problem [18–20]). This means that if more than one stable post buckling state exists, it is conceivable that the state that will be reached after the jump is dependent on the conditions that define the motion at the start of the jump. Consequently, if these conditions are purely artificial, i.e. completely remote from the actual physics of the problem, the outcome of the computations can also be remote from what is observed in practice. Note that this observation, if correct, shed doubts on the possibility of making use of a simpler transient method than the one that was used here (for example the methods that were proposed in [21–23]).

It is thus by no means certain that agreement between experiment and numerical simulation will result from this type of computation. We expect it to depend on how close the numerical model fits into the real data. For example, in both cases discussed in the previous sections, no account was given of the influence of the testing machine. Testing machines absorb elastic energy when the test specimen is loaded. The release of this energy during the jumps has influence on the transient response of the test specimen and thus could have influence on the final state that the structure will reach.

Consequently, one should always be aware of the fact that there are differences between the actual

structure in practice and the models that are produced after them. In the case of buckling problems these differences only need to be slight to cause large differences in behavior between the actual object and the numerical model. This is typical of most buckling problems and the extension of our computational capabilities by the mode jump procedure cannot really alleviate this difficulty.

7. Conclusion

We have no doubts that mode jumping and the more particular case of (simple) collapse can also be simulated by the exclusive use of a transient method, as was already proposed many years ago [24]. However, a solution procedure of this type should preferably be equipped with a variable time step algorithm that is capable of dealing with the sudden change of the rate of deformation at the points where the quasi static behavior goes over to transient behavior, or the other way around. Moreover, it would also be desirable to have a provision that delivers information about the character of the critical points etc. that are passed during the computations. To the best of our knowledge, such procedures are not yet in existence.

In contrast, the procedure discussed in this paper can be applied using existing finite element codes with no need for particular alterations to the code. A basic necessity is the availability of a continuation method and a transient method (and a good shell model). If these methods are available, the calculations can simply be carried out in an interactive mode whereby the change from the static to the transient mode is accomplished through a (default) restart procedure. The procedure is thus based on exploitation of the particular suitability of each separate mode of operation for each separate (static, transient) part of the solutions. As it is shown, this strategy is easy to apply and it presents a considerable enlargement of our simulation capabilities in stability calculations.

Acknowledgments

We thank Professor D. Shilkrut for his interest, mental support and many helpful suggestions. We are also grateful to Mr. G. Rebel for carefully checking the derivations in the manuscript.

Appendix A

The difference between limit points and bifurcation points can be treated on the basis of pure geometrical concepts without reference to the notion of stability. An analysis in this spirit begins with the definitions of these special points of the solutions of the equilibrium equations (Eq. (2))

A limit point:

$$\begin{aligned} \mathbf{x}'_c &= \frac{d\mathbf{x}\langle s_c \rangle}{ds} = \text{single valued} \\ \lambda'_c &= \frac{d\lambda\langle s_c \rangle}{ds} = 0; \quad \lambda''_c = \frac{d^2\lambda\langle s_c \rangle}{ds^2} < 0 \end{aligned} \tag{A.1}$$

Bifurcation point:

$$\mathbf{x}'_c = \frac{d\mathbf{x}}{ds} = \text{multiple valued} = \mathbf{x}'_{c1}, \mathbf{x}'_{c2}, \mathbf{x}'_{c3}, \text{ etc.} \tag{A.2}$$

The equations that determine the unit tangent \mathbf{x}' along $\mathbf{x}\langle s \rangle$ are given by the first derivative of the equilibrium equations

$$(i) \quad \mathbf{f}_x\langle \mathbf{x} \rangle \mathbf{x}' = 0 \quad \{ \mathbf{f}_d\langle \mathbf{d}, \lambda \rangle \mathbf{d}' + \mathbf{f}_\lambda\langle \mathbf{d}, \lambda \rangle \lambda' = 0 \}$$

$$\mathbf{F}_x \langle \mathbf{x} \rangle \mathbf{x}' = \mathbf{e}_{N+1}; \quad (\text{A.3})$$

$$\text{(ii) } \mathbf{x}'^T \mathbf{x}' = 1 \quad \{ \mathbf{d}' \langle \mathbf{d}, \lambda \rangle^T \mathbf{d}' \langle \mathbf{d}, \lambda \rangle + \lambda' \langle \mathbf{d}, \lambda \rangle \lambda' \langle \mathbf{d}, \lambda \rangle = 1 \}$$

The extra equation (ii) defines s as the arclength. Note that the unit vector \mathbf{e}_{N+1} is the base vector that corresponds to λ in the space R_{N+1} .

The Jacobian \mathbf{F}_x of this augmented set of equations is thus

$$\mathbf{F}_x = \begin{Bmatrix} \mathbf{K} & \mathbf{f}_\lambda \\ \mathbf{d}'^T & \lambda' \end{Bmatrix} \in R_{N+1} \times R_{N+1} \quad (\text{A.4})$$

It is now noted that

I: At a *limit point*, Eq. (A.3) must have a unique solution so that

$$\text{Rank}\{\mathbf{F}_x(\mathbf{x}_c)\} = \text{Rank}\{\mathbf{F}_x \langle \mathbf{x}_c \rangle; \mathbf{e}_{N+1}\} = N + 1 \quad (\text{A.5})$$

In that case, Eq. (A.3) reduces to

$$\begin{aligned} \mathbf{K} \langle \mathbf{d}_c, \lambda_c \rangle \mathbf{d}'_c &= 0 \quad (\mathbf{K} = \mathbf{f}_d) \\ \mathbf{d}'_c{}^T \mathbf{d}'_c &= 1 \end{aligned} \quad (\text{A.6})$$

The tangent to the path at the limit point is thus determined by an eigenvalue problem, i.e.

$$\begin{aligned} \mathbf{K} \langle \mathbf{x}_c \rangle \mathbf{a} \langle i \rangle - \omega \langle i \rangle \mathbf{a} \langle i \rangle &= 0 \\ \omega \langle 1 \rangle &= 0: \quad \overline{\omega \langle i \rangle \neq 0} \quad \text{for } i = 2, 3, 4, \dots \\ \mathbf{a} \langle i \rangle^T \mathbf{a} \langle j \rangle &= \delta_{ij}; \\ \mathbf{d}'_c &= \mathbf{a} \langle 1 \rangle \end{aligned} \quad (\text{A.7})$$

The tangent (or path derivative) \mathbf{x}'_{c1} at a limit point is determined by the null vector $\mathbf{a} \langle 1 \rangle$ of the singular $\mathbf{K} \langle \mathbf{x}_c \rangle$. Note that apart from its sign, \mathbf{x}'_{c1} is a unique solution of Eq. (A.3) in this case and that the (augmented) Jacobian \mathbf{F}_x , (A.4), is non-singular at \mathbf{x}_c .

We can now state an important observation. A limit point is a point of the solutions of (2) where the Jacobian \mathbf{K} = singular. But a limit point is not automatically a critical point in the sense of the stability theory. The coincidence only occurs if the path $\mathbf{x} \langle s \rangle$ changes stability at \mathbf{x}_c . Only in that case does condition (A.7) (with $\overline{\omega \langle i \rangle > 0}$ for $i > 1$), indicate that \mathbf{K} is semi-positive definite (14).

II. We now turn to the second type of points.

At a *bifurcation point* we have

$$\text{Rank}\{\mathbf{F}_x \langle \mathbf{x} \rangle\} = \text{Rank}\{\mathbf{F}_x \langle \mathbf{x} \rangle; \mathbf{e}_{N+1}\} = N - K + 1 \quad (\text{A.8})$$

Here, $K + 1$ determines the dimension of the tangent space in which the directions of all the branches \mathbf{x}'_{ci} are defined. But, as before, we will restrict the considerations to simple bifurcation points thus $K = 1$, $\text{Rank}\{\mathbf{F}_x \langle \mathbf{x} \rangle\} = N$.

It is of interest to note that it is possible to deduce from (A.4) that the loss of rank of \mathbf{F}_x , coincides with that of \mathbf{K} and $\mathbf{f}_x = \{\mathbf{K}; \mathbf{f}_\lambda\}$ by the same degree [12, 13]

$$\text{Rank}\{\mathbf{K} \langle \mathbf{x}_c \rangle\} = \text{Rank}\{\mathbf{K} \langle \mathbf{x}_c \rangle; \mathbf{f}_\lambda\} = N - K = N - 1 \quad (\text{A.9})$$

This means that at a bifurcation point \mathbf{K} is again singular with an eigenvector $\mathbf{a} \langle 1 \rangle$ that satisfies

$$\mathbf{a} \langle 1 \rangle^T \mathbf{K} \langle \mathbf{x}_c \rangle = 0; \quad \mathbf{K} \langle \mathbf{x}_c \rangle \mathbf{a} \langle 1 \rangle = 0; \quad \mathbf{a} \langle 1 \rangle^T \mathbf{f}_\lambda \langle \mathbf{x}_c \rangle = 0 \quad (\text{A.10})$$

Please observe that in geometrical terms, the eigenvector $\mathbf{a} \langle 1 \rangle$ represents the difference between the path derivatives of the two paths 1, 2 that are crossing at \mathbf{x}_c (when measured in the plane $\lambda = \lambda_c$).

Also in this case, the bifurcation condition (A.10) does not imply that \mathbf{x}_c is a critical state. This coincidence only happens when one of the bifurcating branches changes stability at \mathbf{x}_c , and thus

$\mathbf{K}\langle \mathbf{x}_c \rangle$ = semi positive definite; $\omega\langle i \rangle > 0$ for $i > 1$ in (A.7).

To determine the derivatives \mathbf{x}'_{c1} , \mathbf{x}'_{c2} at \mathbf{x}_c we can follow several approaches [12–14]. If the tangent \mathbf{x}'_{c1} is calculated *during the course of the computations towards \mathbf{x}_c* , (which happens in most path-following methods), one has the identity

$$\mathbf{F}_{x1}\langle \mathbf{x}_c \rangle \mathbf{x}'_{c1} = \mathbf{e}_{N+1}$$

where

$$\mathbf{F}_{x1} = \begin{Bmatrix} \mathbf{K}\langle \mathbf{x}_c \rangle & \mathbf{f}_k\langle \mathbf{x}_c \rangle \\ (\mathbf{d}'_{c1})^T & \lambda'_{c1} \end{Bmatrix} \quad (\text{A.12})$$

Note that \mathbf{x}'_{c1} is a unit vector in this formulation and also that \mathbf{F}_{x1} = singular with the eigen vectors \mathbf{c} and \mathbf{a} : that belong to its (single) zero eigenvalue given by

$$\begin{aligned} \mathbf{F}_{x1} \mathbf{c} &= 0; & \mathbf{F}_{x1}^T \mathbf{a} &= 0 \\ \mathbf{a} &= \mathbf{a}\langle 1 \rangle = \begin{bmatrix} \mathbf{a}\langle 1 \rangle \\ 0 \end{bmatrix}; & \mathbf{c} &= \mathbf{c}\langle 1 \rangle = \frac{1}{\sqrt{1-\alpha^2}} \{ \mathbf{x}'_{c1} - \alpha \mathbf{a} \} \end{aligned} \quad (\text{A.13})$$

$$\alpha = \mathbf{a}^T \mathbf{x}'_{c1} \quad ^5$$

The tangent \mathbf{x}'_{c2} of the other path going through \mathbf{x}_c , can also be determined from (A.12)

$$\mathbf{F}_{x1}\langle \mathbf{x}_c \rangle \mathbf{x}'_{c2} = \mathbf{e}_{N+1} \quad (\text{A.14})$$

provided \mathbf{x}'_{c1} is not perpendicular to \mathbf{x}'_{c2} . Notice that this vector is not a unit vector because $(\cdot)' = d/ds_1$ means differentiation with respect to s_1 and not with respect to s_2 (=the arc length of branch 2).

To determine the second derivative (in terms of a unit vector) it is better to use the modification of (A.14)

$$\begin{aligned} \mathbf{F}_{x1}\langle \mathbf{x}_c \rangle \mathbf{x}'_{c2} &= \frac{ds_1}{ds_2} \mathbf{e}_{N+1} = \cos \theta \mathbf{e}_{N+1} \\ \mathbf{x}'_{c2} &= \frac{d\mathbf{x}_{c2}}{ds_2}; & (\cdot)' &= \frac{d(\cdot)}{ds_2} \end{aligned} \quad (\text{A.15})$$

where θ is the angle between \mathbf{x}'_{c1} and \mathbf{x}'_{c2} . The solution for \mathbf{x}'_{c2} follows then from

$$\mathbf{x}'_{c2} = [\cos \theta \mathbf{x}'_{c1} + \sin \theta \mathbf{c}\langle 1 \rangle] \quad (\text{A.16})$$

where θ is determined by the non-zero root of the compatibility condition

$$\begin{aligned} \mathbf{a}^T \frac{d^2}{ds^2} \{ \mathbf{F}\langle \mathbf{x}_1 \langle s \rangle \rangle \} &= 0 \\ \Downarrow \\ \mathbf{a}^T [2\mathbf{F}_{xx}\langle \mathbf{x}_c \rangle \mathbf{x}'_{c1} \mathbf{c} \sin \theta \cos \theta + \mathbf{F}_{xx}\langle \mathbf{x}_c \rangle \mathbf{c} \mathbf{c} \sin^2 \theta] &= 0 \end{aligned} \quad (\text{A.17})$$

(The correctness of the formulation presented here can be checked by back substitution (see also [12]).

Notice that the solution for \mathbf{x}'_{c1} in the case of a limit point is completely determined by the linearized equation (A.13) but that in the case of a bifurcation point the second derivative of the equilibrium equations are required (Eq. (A.17)) to find \mathbf{x}'_{c2} . It is finally noted that the above derivation of the direction \mathbf{x}'_{c2} can be used as the basis of a switch procedure between branches at simple bifurcation points.

⁵ This formulation is invalid for $\kappa = 1$, but we prefer to ignore this special case here.

References

- [1] M. Stein, Loads and deformations of buckled rectangular plates, NASA Technical Report R-40, National Aeronautics and Space Administration, 1959.
- [2] M. Stein, The phenomenon of change of buckling patterns in elastic structures, NASA Technical Report R-39, National Aeronautics and Space Administration, 1959.
- [3] W.J. Supple, Changes of wave-form of plates in the post-buckling range, *Int. J. Solids Struct.* 6 (1970) 1243–1258.
- [4] T. Nakamura and K. Uetani, The secondary buckling and post-buckling behaviours of rectangular plates, *Int. J. Mech. Sci.* 21 (1979) 265–286.
- [5] H. Suchy, H. Troger and R. Weiss, A numerical study of mode jumping of rectangular plates, *ZAMM Z. Angew. Math. u. Mech.* 65(2) (1985) 71–78.
- [6] D. Schaeffer and M. Golubitsky, Boundary conditions and mode jumping in the buckling of a rectangular plate, *Commun. Math. Phys.* 69 (1979) 209–236.
- [7] M. Golubitsky and D. Schaeffer, *Singularities and Groups in Bifurcation Theory, Volume I, Applied Mathematical Sciences* (Springer Verlag, New York, Heidelberg, Tokyo, 1985).
- [8] W.T. Koiter, On the stability of elastic equilibrium (H.J. Paris Publ., Amsterdam 1945), English translation: Report No. AFFDL-TR-70-25, Air Force Flight Dynamics Lab., Wright Patterson AFB, OH, 1970.
- [9] W.T. Koiter, Elastic stability and post-buckling behavior, in: R.E. Langer ed., *Proc. Symp. on Nonlinear Problems*, University of Wisconsin Press, 1963, p. 257.
- [10] J.M.T. Thompson and G.W. Hunt, *A General Theory of Elastic Stability* (John Wiley, Chichester, New York, 1973).
- [11] B. Budiansky, Theory of buckling and postbuckling of elastic structures, in: C.S. Yih, ed., *Advances in Applied Mechanics* Vol. 14 (Academic Press, New York, 1974).
- [12] E. Riks, F.A. Brogan and C.C. Rankin, Aspects of the stability analysis of shells. International Conference of Computational Engineering Science, April 10–14, 1988, Atlanta, in: W. B. Krätzig and E. Oñate, eds., *Static and Dynamic Stability of Shells, Springer Series in Computational Mechanics* (Springer Verlag, Heidelberg, 1990).
- [13] E. Riks, Progress in collapse analysis, *J. Pressure Vessel Technol.* 109 (1987) 27–41.
- [14] E. Riks, Some computational aspects of the stability analysis of nonlinear structures, *Comput. Methods Appl. Mech. Engrg.* 47 (1984) 219–259.
- [15] C. Rankin et al., The STAGS user's manual, NASA CONTRACTOR REPORT, to be published.
- [16] K.C. Park, Evaluating time integration methods for nonlinear dynamic analysis, in: T. Belytschko, J.R. Osias and P.V. Marcal, eds., *Finite Element Analysis for Transient Nonlinear Behavior, Applied Mechanics Symposia Series* (ASME, New York, 1975).
- [17] C.C. Rankin, E. Riks, J.H. Starnes and W. Allen Waters, Jr., An experimental and numerical verification of the postbuckling behavior of a composite cylinders in compression, NASA CONTRACTOR REPORT, to be published.
- [18] D. Shilkrut, Investigation of axisymmetric deformation of geometrically non-linear, rotationally, orthotropic, circular plates, *Int. J. Non-Linear Mech.* 18(2) (1983) 95–118.
- [19] D. Shilkrut, Stability and vibration of geometrically nonlinear cylindrically orthotropic circular plates, *J. Appl. Mech.* 51 (1984) 345–360.
- [20] D. Shilkrut, The influence of the paths of multiparametrical conservative loading on the behaviour of a geometrically nonlinear deformable elastic body, in: I. Elishakoff, J. Arboz, C.D. Babcock, Jr. and A. Libai, eds., *Buckling of Structures; Theory and Experiment. The Joseph Singer Anniversary Volume* (Elsevier, 1988).
- [21] B.H. Kröplin and D. Dinkler, A creep type strategy used for tracing the load path in elastoplastic postbuckling analysis, *Comput. Methods Appl. Mech. Engrg.* 32 (1982) 365–376.
- [22] B.H. Kröplin and D. Dinkler, Eine Methode zur directen Berechnung von Gleichgewichtslagen im Nachbeul-bereich, *Ingenieur Archiv* 51 (1982) 415–420.
- [23] C. Petiau and C. Cornuault, Efficient algorithms for post buckling computations, in: R. Glowinsky and J.L. Lions, eds., *Computing Methods in Applied Science and Engineering* (Elsevier, North Holland, Amsterdam, 1984).
- [24] V.I. Feodos'ev, On a method of solution of the nonlinear problems of stability of deformable systems, *PPM* (2) (1963) 265–274.